

# Chapter 4

## Simulation of tides in the Bay of Bengal

---

### 4.1 Introduction

The magnitude and extent of severity of storm surges produced along a coast due to a tropical cyclone not only depends on the magnitude of meteorological forcing but also depends on the phase of tide at that location. The worst disasters occur when large surges coincide with high tide [Murty et al., 1986; Flather, 1994]. The real magnitude of storm surges can be predicted accurately only if the interaction between tides and surges are taken into account. Therefore, as a first step towards simulating the combined effect of tides and surges, it is useful to develop a model driven by tides alone [Jones and Davies, 2005], which can be efficiently validated with locally available tide gauge records. The tidal model can, then, be modified to incorporate meteorological forcing to simulate storm surges.

In addition, the tidal model can be used to extract the amplitudes and phase of tidal constituents, which are useful to predict high and low tides at a place. As mentioned in Section 1.5, the attempts made to understand the characteristics of tides in the Bay of Bengal are very limited. Murty and Henry [1983] developed co-tidal charts of major tidal constituents  $M_2$ ,  $S_2$ ,  $K_1$ , and  $O_1$  in the Bay with the aid of numerical model. The model was driven by tidal elevations prescribed along the southern open boundary of the model obtained by linear interpolation of widely separated tidal observations in Sri Lanka, the Nicobar Islands and Thailand, as there was lack of information on tidal elevations in the deep regions.

Fortunately with the advent of satellite altimeter since 1992, the present global tidal models, which assimilate altimetry data, can provide reliable information on tides in oceans, except very near the coast. The global tidal models

can be used to extract composite tidal elevations as well as the amplitudes and phases of the tidal constituents at relatively deep locations.

This chapter describes the simulation of tides in the Bay of Bengal and validation of tidal model. As evident from Figure 1.2, the major semi-diurnal and diurnal constituents that have relatively high amplitudes are  $M_2$ ,  $S_2$ ,  $N_2$  and  $K_1$ ,  $O_1$ , respectively. Separate simulations were carried out for each of these major tidal constituents in order to generate co-tidal and co-range charts for the Bay of Bengal, which is also described in this Chapter.

## **4.2 Data and methodology**

### **4.2.1 Global Tidal Model - FES2004**

The present global tidal models, developed by assimilating altimetric data obtained from TOPEX/Poseidon (T/P), are found to perform better than the earlier models of Schwiderski [1980] and Cartwright and Ray [1991] [Andersen et al., 1995], with significant improvement in deep ocean (ocean depth greater than 1000 m) where the accuracy approaches that of tidal analysis method [Shum et al., 1997]. Shum et al. [1997] compared ten global models developed prior to 1997 and showed that the models agreed within 2-3 cm in deep ocean (where ocean depth is greater than 800 m). Among the different T/P based models, Shum et al. [1997] recommended CSR3.0 [Eanes and Bettadpur, 1996] and FES95.2.1 [Le Provost et al., 1998] models to be superior to other global models.

The FES (Finite Element Solution) global tidal model series were developed by Christian Le Provost [Le Provost et al., 1994]. FES2004 [Lyard et al., 2006] is the latest version preceded by FES99 [Lefevre et al., 2002], FES98 [Lefevre et al., 2000], FES95.2.1, and FES94 [Le Provost et al., 1994]. Tide gauge data from several data banks and altimeter dataset from TOPEX/Poseidon and ERS-2 were assimilated into the FES2004 to improve the accuracy of the solutions. The other improvements of FES2004 solution over FES99 are refinement of element mesh up to  $1/8^\circ$  grid resolution, inclusion of  $S_1$  tide from Richard Ray and inclusion of four long hydrodynamic period waves [Lyard et al., 2006]. Additionally, FES2004

data package includes prediction code through which composite tidal elevations can be easily extracted at required grid points for any time period along the open boundary of regional model.

In the FES2004 datasets, though documented to be the most accurate among the FES series, ambiguity in the tidal solutions in coastal and shelf regions still persist [Lyard et al., 2006]. Subeesh [2010] evaluated the accuracy of tidal constituents obtained from two global tidal models FES2004 and OTPS [Egbert and Erofeeva, 2002] for the Indian Ocean. The author computed the root mean square error (RMSE) for the two global models between the predicted and observed tides at three island stations in the equatorial Indian Ocean and three coastal stations in the Arabian Sea. Subeesh [2010] concluded that the RMSE for the major tidal constituents obtained from FES2004 were less than that obtained from OTPS by 15% at most of the stations, except at two stations where the RMSE for FES was higher by 3%.

Figures 4.1 to 4.5 show the distribution of amplitude and phase of the major tidal constituents  $M_2$ ,  $S_2$ ,  $N_2$ ,  $K_1$  and  $O_1$  in the Bay of Bengal obtained from the FES2004 datasets. The discrepancies in the FES solutions near the coastal areas are evident from the scatter plots (Figure 4.6) of the amplitudes of major tidal constituents from FES2004 dataset and the amplitudes obtained from the Admiralty Tide Table (ATT) at different stations along the coast of Bay of Bengal whose locations are tabulated in Table 4.1. The highly scattered values show that FES2004 is unable to provide accurate solutions at most of the coastal stations.

Lyard et al. [2006], in order to increase the accuracy of tidal prediction in shallow waters, emphasized on the development of high resolution regional tidal models which can accurately reproduce the tidal dynamics on shelves and shallow regions. In the last few decades, a few regional models have been developed which utilized the tidal elevations extracted from FES global model to prescribe the open boundary conditions. Jarosz et al. [2005], in order to describe the tidal characteristics of Bab el Mandeb Strait, developed a barotropic model which was driven by tidal elevations generated from tidal harmonic constituents extracted from FES95.2. Unnikrishnan et al. [1999] studied the propagation of tides in the

Gulf of Khambhat and Bombay High regions using tidal model driven by harmonic constituents extracted from FES94.

**Figure 4.1** Distribution of amplitude and phase of  $M_2$  tide in the Bay of Bengal obtained from FES2004 as a) co-range lines and b) co-tidal lines. Amplitudes are given in centimetres and phase  $G$  is given in degrees.

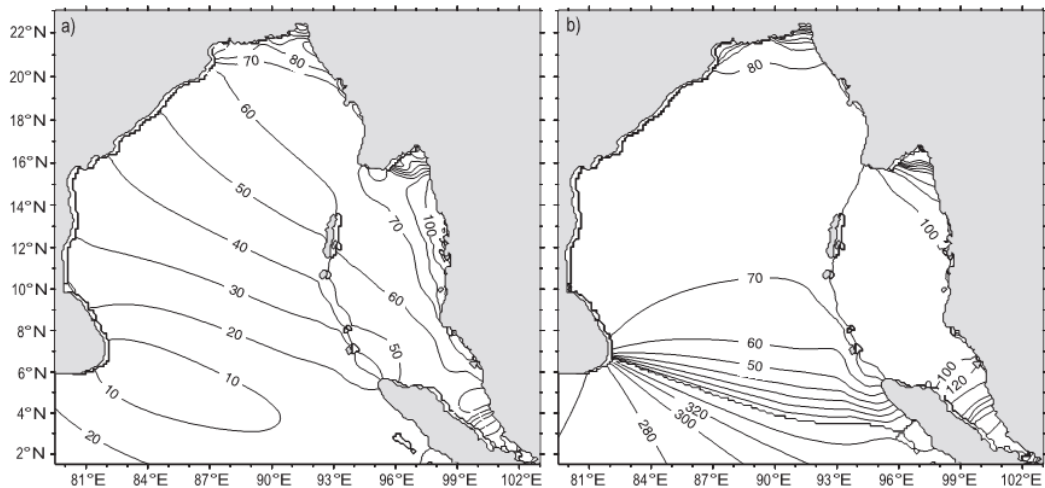


**Figure 4.2** Distribution of amplitude and phase of  $S_2$  tide in the Bay of Bengal obtained from FES2004 as a) co-range lines and b) co-tidal lines. Amplitudes are given in centimetres and phase  $G$  is given in degrees.

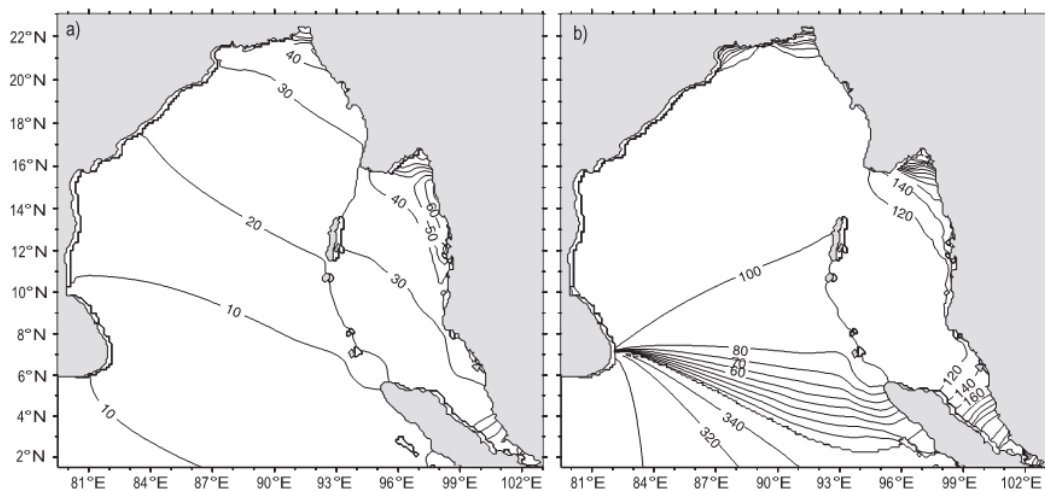


**Figure 4.3** Distribution of amplitude and phase of  $N_2$  tide in the Bay of Bengal obtained from FES2004 as a) co-range lines and b) co-tidal lines. Amplitudes are given in centimetres and phase  $G$  is given in degrees.

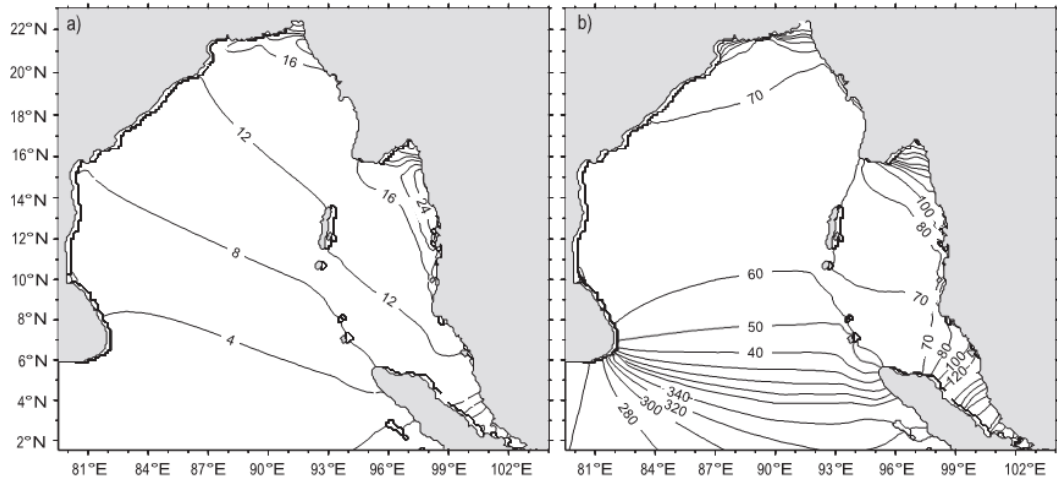


**Figure 4.4** Distribution of amplitude and phase of  $K_1$  tide in the Bay of Bengal obtained from FES2004 as a) co-range lines and b) co-tidal lines. Amplitudes are given in centimetres and phase  $G$  is given in degrees.

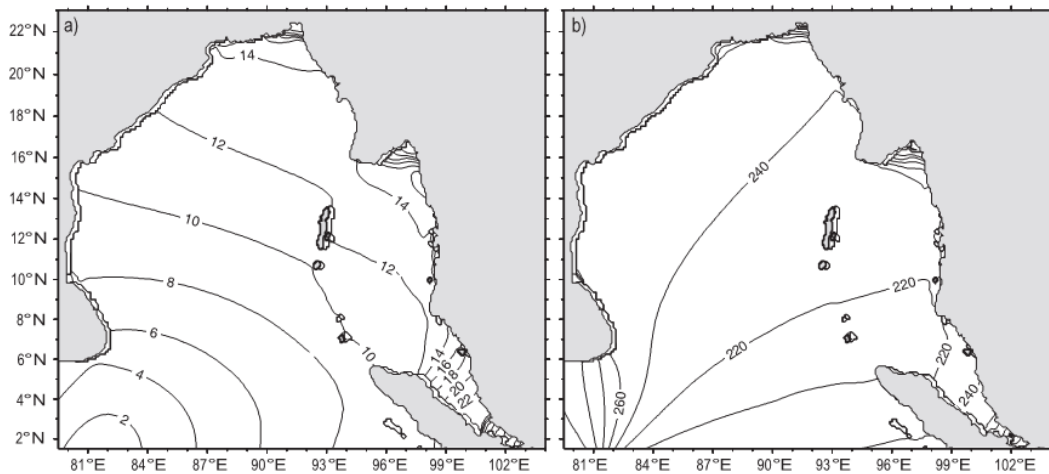
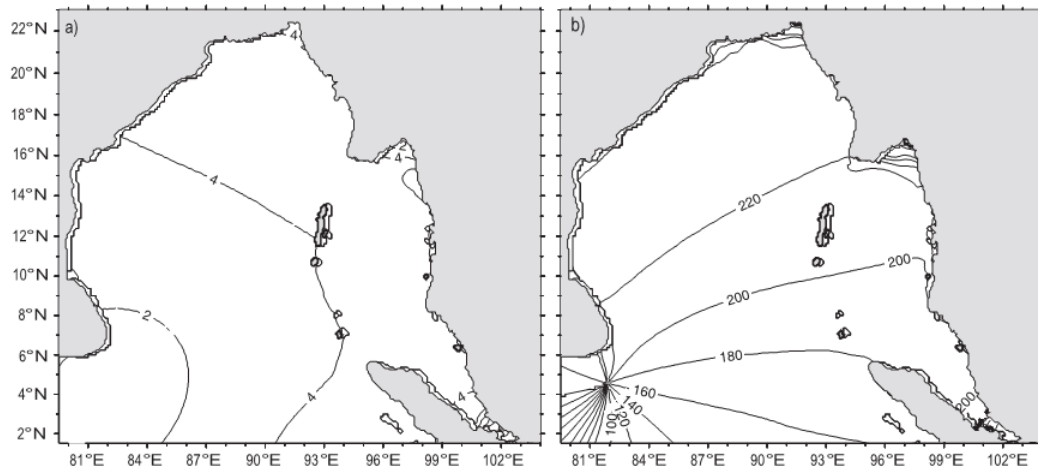


**Figure 4.5** Distribution of amplitude and phase of  $O_1$  tide in the Bay of Bengal obtained from FES2004 as a) co-range lines and b) co-tidal lines. Amplitudes are given in centimetres and phase  $G$  is given in degrees.



#### 4.2.2 Tidal Model for the Bay of Bengal

In the present study, two different numerical experiments were carried out:

- i. Simulation of composite tides
- ii. Simulation of each of the five major tidal constituents  $M_2$ ,  $S_2$ ,  $N_2$ ,  $K_1$  and  $O_1$ .

The data and methodology adopted for these simulations are described in this section. The hydrodynamic equations and the numerical techniques used to solve the equations are presented in Section 2.2 and 2.4, respectively. The numerical solution of the equations is obtained by discretizing the equations in space using an explicit finite difference scheme over a uniformly staggered Arakawa-C grid and in time using leap-frog technique. The model domain covering the entire Bay of Bengal, including Andaman Sea and Malacca Strait, with north-south extension from 1.5°N to 23°N and east-west extension from 79.8°E to 103°E is shown in Figure 4.7.

**Figure 4.6** Scatter plot of the amplitudes of tidal constituents a)  $M_2$ , b)  $S_2$ , c)  $K_1$ , and d)  $O_1$  extracted from FES2004 dataset and that obtained from Admiralty Tide Table at different stations along the coast of Bay of Bengal (locations tabulated in Table 4.1 and shown in Figure 4.7). The stations located in different regions (regions categorized as per Table 4.1) are marked with different symbols.

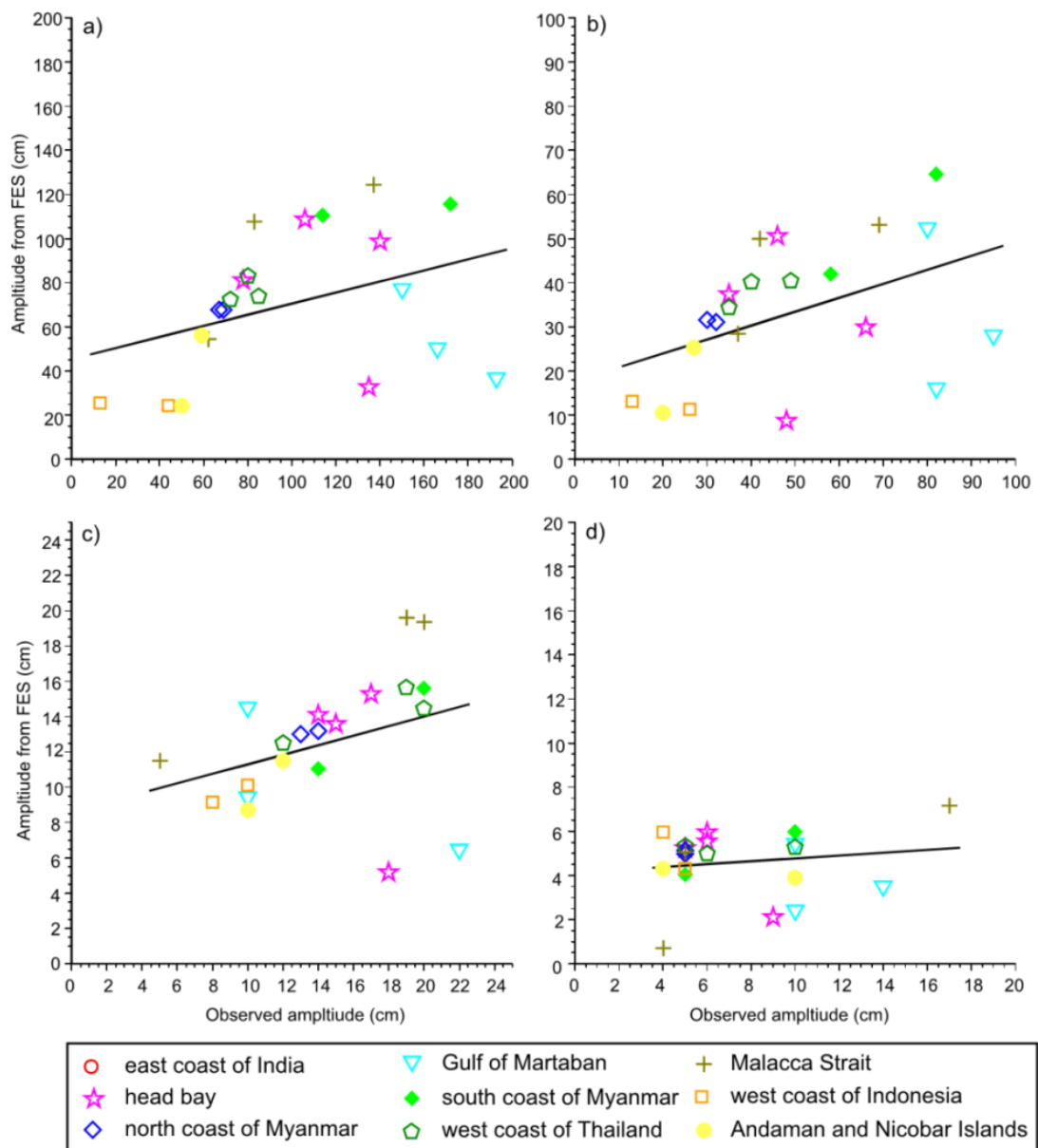


**Figure 4.7** Model domain showing the 5 min (approximately 9.2 x 9.2 km) computational grid and the location of 114 stations at which the simulated tidal elevations were extracted. The stations include the 13 Standard Ports (circles) and 31 Secondary Ports (stars) at which the model derived tidal constituents are compared with the observed constituents. The names of the Standard and Secondary Ports are referred in Table 4.1. The dashed lines represent the two southern open boundaries along 1.5°N and the western open boundary along 79.8°E. The coastlines of the seven countries bordering the Bay of Bengal and the four maritime states along the east coast of India are highlighted with different colours.

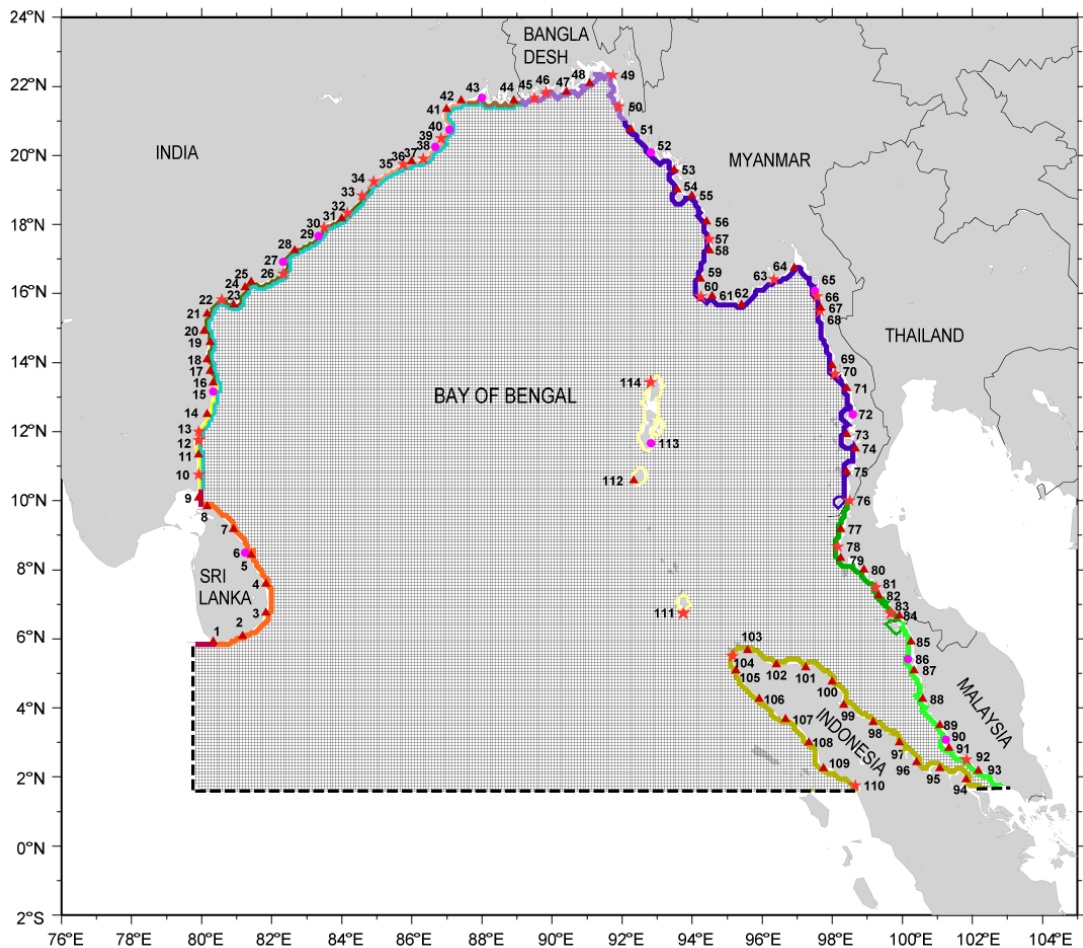




**Table 4.1** The name and location of 13 Standard Ports (bold) and 31 Secondary Ports as documented in Indian Tide Table and Admiralty Tide Table, respectively. The Time Zone and the height of Mean Sea Level (MSL) with respect to Chart Datum (CD) at each Port are also tabulated. The longitude and latitude of the grid points closest to location of station and the depth at that point in the model domain is also shown.

Country	St No.	Station Name	Longitude (°E) /Latitude (°N)	Time Zone (hours)	MSL (m)	Corresponding Lon(°E) /Lat(°N) in model	Depth (m)
Sri Lanka	<b>6</b>	<b>TRINCOMALEE</b>	<b>81.217, 8.550</b>	<b>-5.30</b>	<b>0.39</b>	81.250, 8.500	24.268
East coast of India	10	Nagapattinam	79.850,10.767	-5.30	0.34	79.917, 10.750	11.026
	12	Cuddalore	79.783, 11.933			79.917, 11.750	16.200
	13	Pondicherry	79.833, 11.933			79.917, 12.000	18.076
	<b>15</b>	<b>CHENNAI</b>	<b>80.300, 13.100</b>	<b>-5.30</b>	<b>0.65</b>	80.333, 13.167	13.318
	22	Surya Lanka	80.533, 15.850			80.583, 15.833	4.932
	26	Sacramento Shoal	82.317, 16.600			82.333, 16.583	13.888
	<b>27</b>	<b>KAKINADA</b>	<b>82.250,16.933</b>	<b>-5.30</b>	<b>0.87</b>	82.333, 16.917	0.293
	<b>29</b>	<b>VISAKHAPATNAM</b>	<b>83.283, 17.683</b>	<b>-5.30</b>	<b>0.84</b>	83.333, 17.667	23.074
	30	Bhimunipatnam	83.450, 17.900			83.500, 17.917	6.650
	32	Kalingapatnam	84.133, 18.350			84.167, 18.333	14.246
	33	Baruva	84.600, 18.867			84.583, 18.833	13.045
	34	Gopalpur	84.917, 19.267			84.917, 19.250	10.158
	35	Chilka Mouth	85.767, 19.717			85.750, 19.750	12.289
	37	Devi River Entrance	86.367, 19.950			86.333, 19.917	17.260
	<b>38</b>	<b>PARADIP</b>	<b>86.683, 20.267</b>	<b>-5.30</b>	<b>1.66</b>	86.667, 20.250	5.791
head bay	39	False Point	86.783, 20.417			86.833, 20.500	9.047
	<b>40</b>	<b>SHORTT ISLAND</b>	<b>87.067, 20.783</b>	<b>-5.30</b>	<b>1.92</b>	87.083, 20.750	2.034
	<b>43</b>	<b>SAGAR ROADS</b>	<b>88.050, 21.650</b>	<b>-5.30</b>	<b>3.00</b>	88.000, 21.667	1.224
	45	Pussur River Entrance	89.467, 21.800	-6.00	1.70	89.500, 21.667	4.741
	46	Tiger Point	89.833, 21.850			89.833, 21.833	0.297
	49	Chittangong	91.833, 22.333			91.750, 22.333	2.282
	50	Cox's Bazar	91.983, 21.433			91.917, 21.417	5.561
north coast of Myanmar	<b>52</b>	<b>AKYAB</b>	<b>92.900, 21.133</b>	<b>-6.30</b>		92.833, 20.083	4.674
	57	Gwa Bay	94.567, 17.583			94.500, 17.583	15.222
	60	Bassein River Entrance	94.267, 15.867	-6.30		94.250, 15.917	3.417
Gulf of Martaban	63	Elephant Point	96.300, 16.500			93.333, 16.417	0.394
	<b>65</b>	<b>AMHERST</b>	<b>97.567, 16.083</b>			97.500, 16.083	5.475
	66	Double Island	97.583, 15.866			97.583, 15.917	10.304
	68	Bentinck Sound	97.683,15.533			97.667,15.500	-8.595

**Table 4.1** Continued

south coast of Myanmar	70	Sinbyubyin	98.250,13.850			98.083,13.667	-5.13
	<b>72</b>	<b>MERGUI</b>	<b>98.600, 12.433</b>	<b>-6.30</b>	<b>2.79</b>	98.583, 12.500	1.545
	76	Pulau Besin	98.483, 9.983			98.500, 10.000	1.183
west coast of Thailand	78	Klong Thung Maphrao	98.250, 8.600			98.167, 8.667	13.134
	81	Ko Ha Hyai	98.900, 7.467			99.250, 7.500	4.719
	83	Pulau Lela	99.700, 6.333			99.667, 6.750	7.285
Malacca Strait	<b>86</b>	<b>PINANG</b>	<b>100.35, 5.417</b>	<b>-8.00</b>	<b>1.69</b>	100.167, 5.417	1.264
	<b>90</b>	<b>PELABUHAN KLANG</b>	<b>101.35, 3.033</b>	<b>-8.00</b>	<b>3.21</b>	101.250, 3.083	10.214
	92	Port Dickson	101.783, 2.517	-8.00	1.50	101.833, 2.500	2.254
west coast of Indonesia	104	Sabang	95.333, 5.833			95.167, 5.500	20.756
	110	Sibolga	98.767, 1.750			98.667, 1.750	13.080
Andaman & Nicobar Islands	111	Galathea Bay	93.850, 6.783			93.750, 6.750	166.000
	<b>113</b>	<b>PORT BLAIR</b>	<b>92.767, 11.683</b>	<b>-5.30</b>	<b>1.21</b>	92.833, 11.667	141.770
	114	Temple Sound	92.850,13.433			92.833, 13.417	3.855

### Bathymetry

The efficiency of a model to simulate tides accurately depends on the extent to which the shallow depths are represented precisely. The role and importance of the real and accurate bathymetry dataset in numerical models to reproduce the observed tidal elevations and currents have been highlighted by Jarosz et al. [2005] and Sinha et al. [2000]. Therefore, the bathymetry for the domain of the tidal model (Bay of Bengal region) was extracted from the improved ETOPO5 dataset (the generation of the dataset and its improvements in shallow regions are described, in detail, in Chapter 3).

The bathymetric contours for the model domain are shown in Figure 4.8. The maximum depth is found to be 6000 m and the minimum depth is assigned as 5 m. The variation in the width of continental shelf is clearly evident from Figure 4.8, with a narrow shelf (30 km) along the east coast of India which widens towards the head bay and along the southern coast of Myanmar, the width being approximately 190 km and 230 km, respectively. The entire Gulf of Martaban is

very shallow with depth less than 50 m while the depth in the Malacca Strait varies from 150 m in the northern part to less than 10 m at the southern end.

### **Schematization**

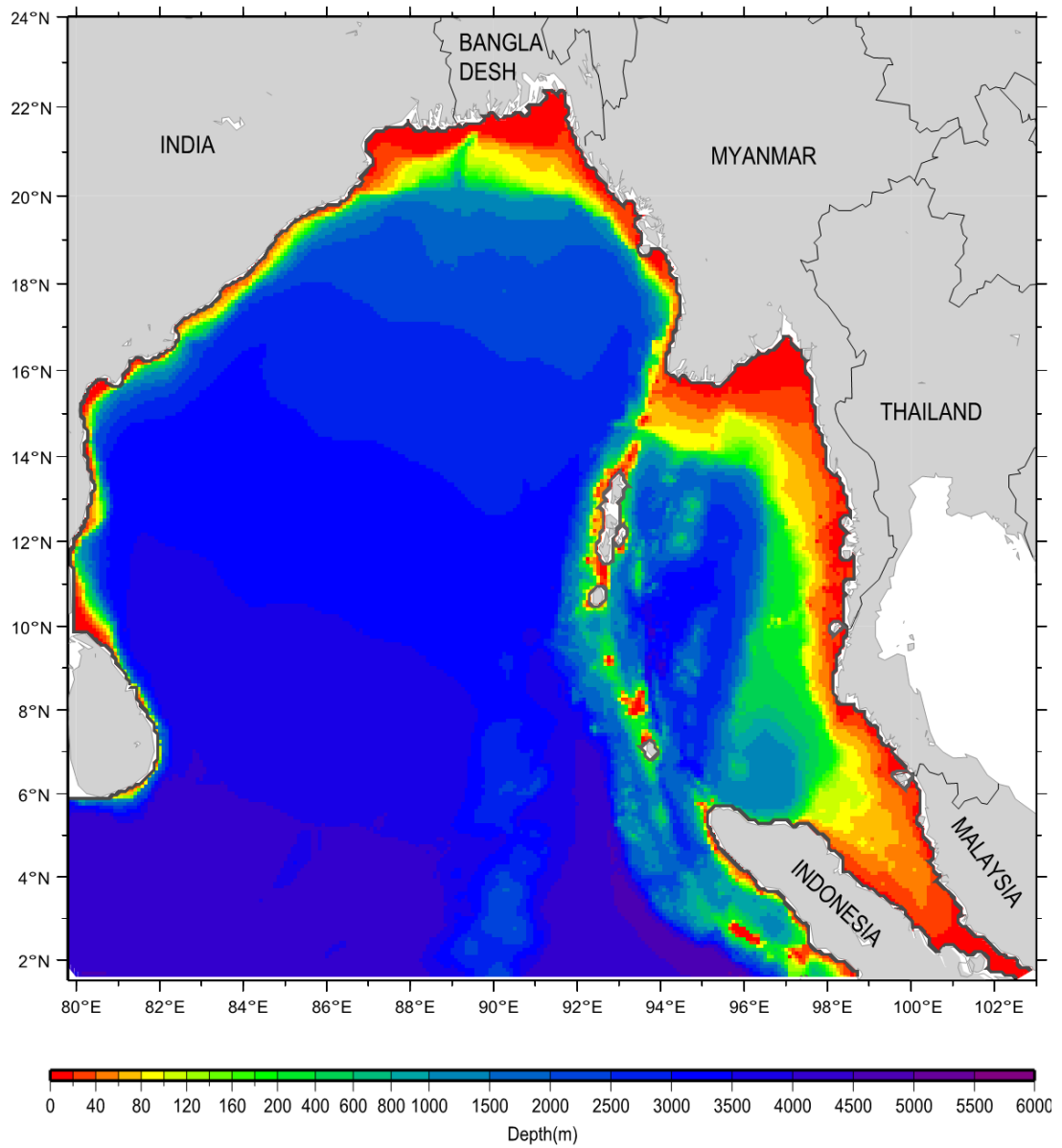
The model domain, covering the entire Bay of Bengal, was schematized on a rectangular mesh with uniform grid spacing of 5 min (approximately 9.2 km) resulting in 278 longitudinal grid points and 258 latitudinal grid points. The CFL criteria was used to determine the time step for a grid spacing of approximately 9.2 km and after some numerical experiments, a time step of 12 sec was chosen.

### **Open boundary conditions**

There are two open boundaries on the southern end of model domain along  $1.5^{\circ}\text{N}$  latitude, separated by the land mass of Indonesia. Both the southern boundaries have east west orientation. The open boundary located to the west of Indonesia consists of 228 grid elements while open boundary to the east of Indonesia (i.e., the open boundary located in the Malacca Strait) consists of 10 grid elements. The western open boundary is located along  $79.8^{\circ}\text{E}$  longitude with north-south orientation consisting of 53 grid elements. The locations of the three open boundaries in the model domain are shown as dashed lines in Figure 4.7.

Along the open boundaries, composite tidal elevations were specified to drive the tidal model. With the aid of prediction code included in the FES2004 dataset, a time series of the composite tidal elevations were obtained at selected grid points, which were then linearly interpolated to obtain the tidal elevations at all grid points along the boundaries. In order to simulate each of the tidal constituents, the amplitude and phase of the respective constituent, extracted from the FES2004 dataset at selected grid points, was used to construct time series for each constituent. These elevations were also linearly interpolated to all grid points along the open boundaries.

**Figure 4.8** Bathymetry for the model domain extracted from Sindhu et al. [2007]. The depths are in metres relative to MSL



**Closed boundary conditions**

The coastline of Bay of Bengal and the coastline around small islands in the Bay, when schematized as stair steps for the tidal model, produced 832 and 108 coastal grid points, respectively. The coastal boundaries were treated as impermeable by imposing zero normal flux and slip conditions at the boundaries as discussed in Section 2.5.2.

**Data used for model validation**

The performance of the tidal model was assessed using the hourly data of observed sea level available from the tide gauges at Chennai, Visakhapatnam, and Paradip for the period 1974-1988.

The model results were also validated against the tidal constituents obtained from Admiralty Tide Table (ATT), Volume 3 published by United Kingdom Hydrographic Office [UKHO, 2000], which provides the amplitude and phase 'g' of semi-diurnal constituents  $M_2$ ,  $S_2$  and the diurnal constituents  $K_1$ ,  $O_1$ . Among the various ports documented in ATT, 44 ports are identified to be within the model domain in which 13 are Standard Ports and 31 are Secondary ports. The geographical locations of these ports are listed in Table 4.1 and displayed in Figure 4.7. The amplitudes and phases of the semi-diurnal constituent  $N_2$  were obtained only at Standard and Secondary Ports along the east coast of India from the Special Publications of International Hydrographic Bureau (IHB), Monaco.

In addition to the observed hourly tidal gauge data, which we could get only at three stations, we used the predicted tidal elevations at 13 Standard Ports that were documented in the Indian Tide Tables (ITT) for comparison. The ITT provides predicted time and height of high and low waters based on continuous observation of tide over a period of one year at Standard Ports. The time associated with tidal prediction at a Standard Port is expressed in the official Local Time adopted at that place and all predicted heights are given in metres above Chart Datum (CD). ITT provides information about the Mean Sea Level (MSL) with respect to Chart Datum and Time Zone, which is the relation between Local Time and Greenwich Mean Time (GMT) for each tide gauge station. The

observed hourly time series obtained from the tide gauges at Paradip, Chennai and Visakhapatnam are also relative to Chart Datum and expressed in Local Time (IST).

The name and location of 44 stations along with the Time Zone and MSL adopted for the 13 Standard Ports covering the coast of India, Bangladesh, Myanmar, Thailand and Malaysia are listed in Table 4.1. Table 4.1 also documents the grid points (longitude and latitude) closest to the location of these 44 stations at which the simulated tidal elevations are stored.

### **4.3 Tuning of the tidal model**

The simulation of tides in the Bay of Bengal was carried out for a period of 3 months so that the time series of simulated tidal elevations is long enough to enable accurate extraction of major semi-diurnal and diurnal constituents through harmonic analysis. Therefore, the tidal elevations were extracted from the FES2004 for a period of 103 days from June 20, 1981 to September 30, 1981 and prescribed along the open boundaries. Though it was experimentally evaluated that the model required 48 hours to spin-up and reach a stable state, the model output was stored from 11<sup>th</sup> day onwards. The investigation carried out by Hall and Davies [2005] implied that the accuracy of the major tidal constituents  $M_2$ ,  $S_2$ ,  $N_2$ ,  $K_1$  and  $O_1$  derived through harmonic analysis of short span data can be improved if the composite tidal elevations are generated from a combined effect of all constituents which includes the higher harmonics and shallow water constituents arising from non-linear interactions and the data are stored every 10 minutes. Therefore, though the time step used in the model was 12 seconds, the simulated composite tide elevations were stored at every 10 minutes for a period of 92 days at 114 grid points along the coast covering almost the entire model domain (Figure 4.7). The 114 stations included the 44 check stations, tabulated in Table 4.1, representing the locations of the Standard/Secondary Ports at which model output was compared with the observed data.

The model was calibrated through fine tuning of friction coefficient,  $C_d$  and eddy viscosity,  $A_H$  in order to achieve maximum agreement between the simulated

and observed tidal elevations. A detailed analysis of the model results obtained from a series of simulations with friction coefficient ranging from 0.001 to 0.003 suggested an improvement in the model results at shallow coastal areas with increasing  $C_d$  values while the tidal elevations in deeper waters (greater than 500 m) appeared to be insensitive to friction coefficient. Therefore, following values were used for  $C_d$  :

$$C_d = 0.0025 \text{ for } h \leq 100,$$

$$C_d = 0.002 \text{ for } 100 < h \leq 500,$$

$$C_d = 0.0015 \text{ for } h > 500.$$

In order to test the sensitivity of tidal model to horizontal eddy viscosity,  $A_H$ , several experiments were carried out for uniform value of  $A_H$  ranging from 1000 to 2000  $\text{m}^2/\text{sec}$ . Though the simulated tidal elevations were not sensitive to the changes in  $A_H$ , relatively better agreement was achieved between observed and simulated elevations for  $A_H = 1500 \text{ m}^2/\text{sec}$ .

## **4.4 Validation of the tidal model**

This section describes the validation of tidal model which was carried out in two different ways, as described in Section 4.2.2:

- Comparison of simulated composite tidal elevations stored at grid points that correspond to locations of Chennai, Visakhapatnam and Paradip with the observed sea level data available at these ports.
- Comparison of the model derived amplitudes and phases of the major tidal constituents at 44 stations with those documented in ATT.

In addition, the composite tidal elevation time series were also compared with the predicted high and low water level data obtained from ITT at 13 Standard Ports.

### **4.4.1 Comparison with observed sea level data**

The simulated composite tidal elevations were compared with the observed tide gauge data at Chennai, Visakhapatnam, and Paradip after shifting the datum from

MSL to CD and making necessary adjustment related to the Time Zone as per the relation listed in Table 4.1.

Figure 4.9 shows the time evolution of simulated and observed tidal elevations for the month of August 1981, covering a spring – neap cycle. It is evident that the mixed semi-diurnal tidal ranges and the spring-neap tidal cycles are well reproduced in the model at all the 3 stations - Chennai, Visakhapatnam and Paradip with a RMSE of 7.20, 6.74 and 7.24 cm, respectively.

#### **4.4.2 Comparison with observed amplitudes and phases of tidal constituents**

The composite tidal elevation time series, obtained from model simulation, was harmonically analyzed using TASK2000 software [Bell et al., 2000], derived from the TIRA tidal analysis program [Murray, 1964] to obtain the amplitude and phase  $G$  of the major semi-diurnal and diurnal constituents (hereafter referred to as model derived constituents). Since the span of the data analyzed was more than 90 days, the major semi-diurnal and diurnal constituents could be extracted accurately [Bell et al., 2000]. The phase ' $G$ ' of each model derived constituent at all stations was converted to include the Local Time Zone effect and obtain phase ' $g$ ' using the Equation (1.2) presented in Section 1.1.4.

Figures 4.10 to 4.13 show the amplitudes and phases of the model derived tidal constituents at 114 stations including the 44 check stations at which the observed data are available. The comparison of the amplitudes of model-derived constituent with the observed indicates that the solution fits quite well with the observations. The model derived constituents  $M_2$  and  $S_2$  show high variation in amplitude and the diurnal constituents  $K_1$  and  $O_1$  show relatively constant amplitudes along the coast of Bay of Bengal, which is in agreement with the observed amplitudes.



**Figure 4.9** Comparison of simulated tidal elevations (cm with respect to CD) (black line) with the observed hourly tidal elevations (red circles) obtained from tide gauge records at a) Paradip, b) Visakhapatnam, and c) Chennai. The predicted high and low water levels obtained from ITT are also shown (blue circles) for comparison. The time 00 hours corresponds to 00 hours on August 01, 1981.

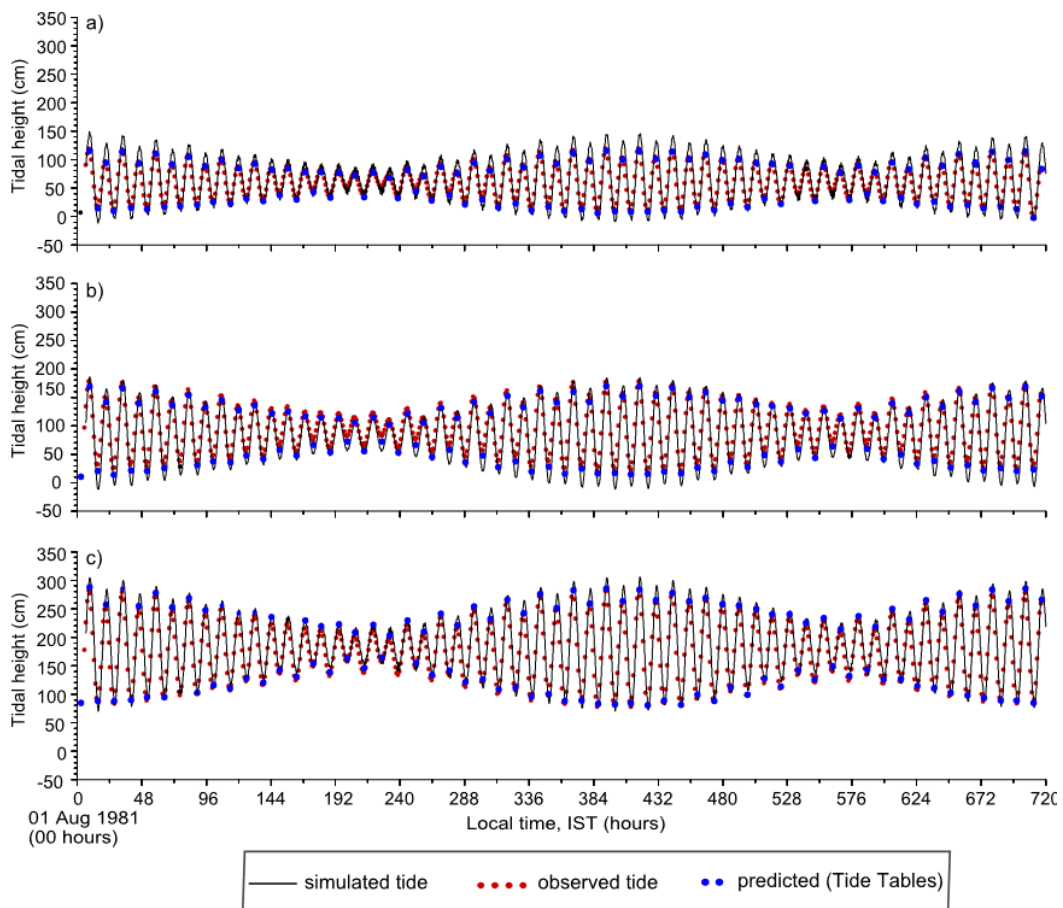


**Figure 4.10** Comparison of the model derived and observed amplitudes of semi-diurnal constituents a)  $M_2$ , b)  $S_2$ , and c)  $N_2$ . The amplitudes of the simulated constituents extracted at 114 stations are shown as continuous line while the observed amplitudes of  $M_2$  and  $S_2$  extracted from ATT at 44 stations are indicated as circles. The observed amplitudes of  $N_2$  tide is obtained only at stations along the east coast of India from IHB. The names of the 44 stations are tabulated in Table 4.1. The abscissa represents the station number assigned to the 114 stations, the locations of which are shown in Figure 4.7.

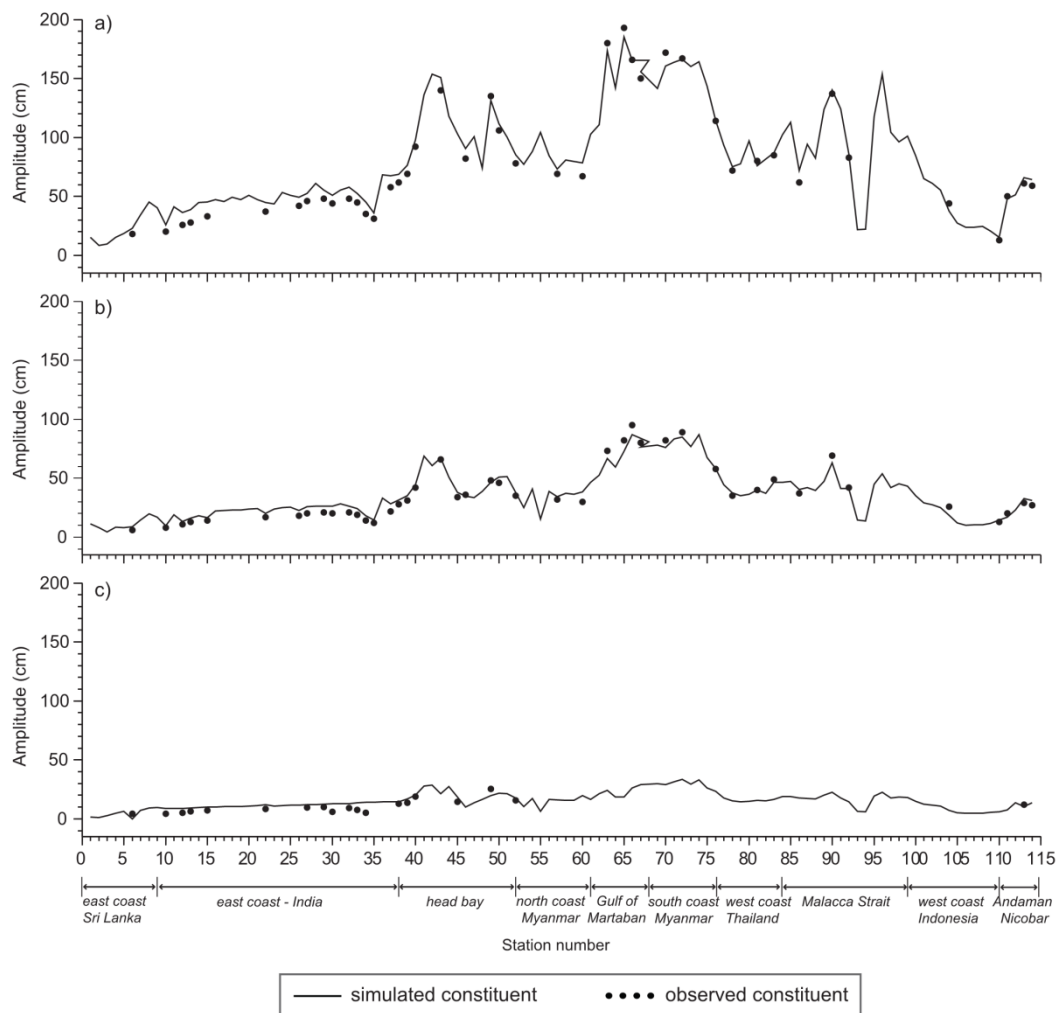


**Figure 4.11** Same as Figure 4.10, but for amplitudes of diurnal constituents, a)  $K_1$  and b)  $O_1$ .

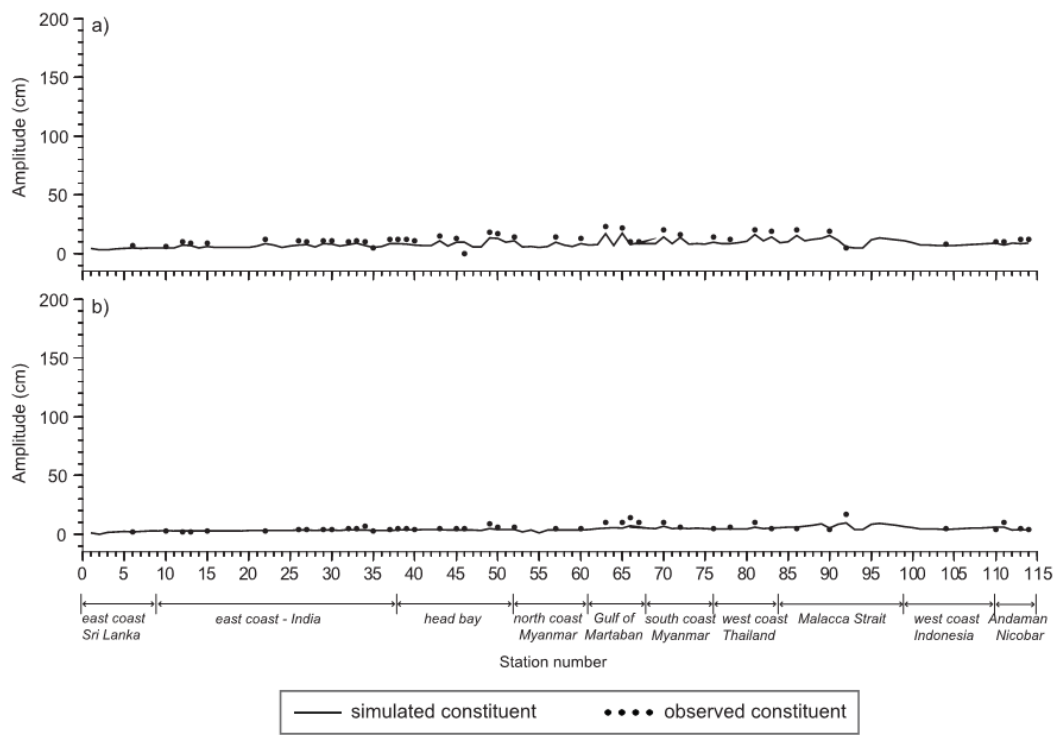


**Figure 4.12** Same as Figure 4.10, but for the phases  $g$  of semi-diurnal constituents a)  $M_2$ , b)  $S_2$ , and c)  $N_2$ .

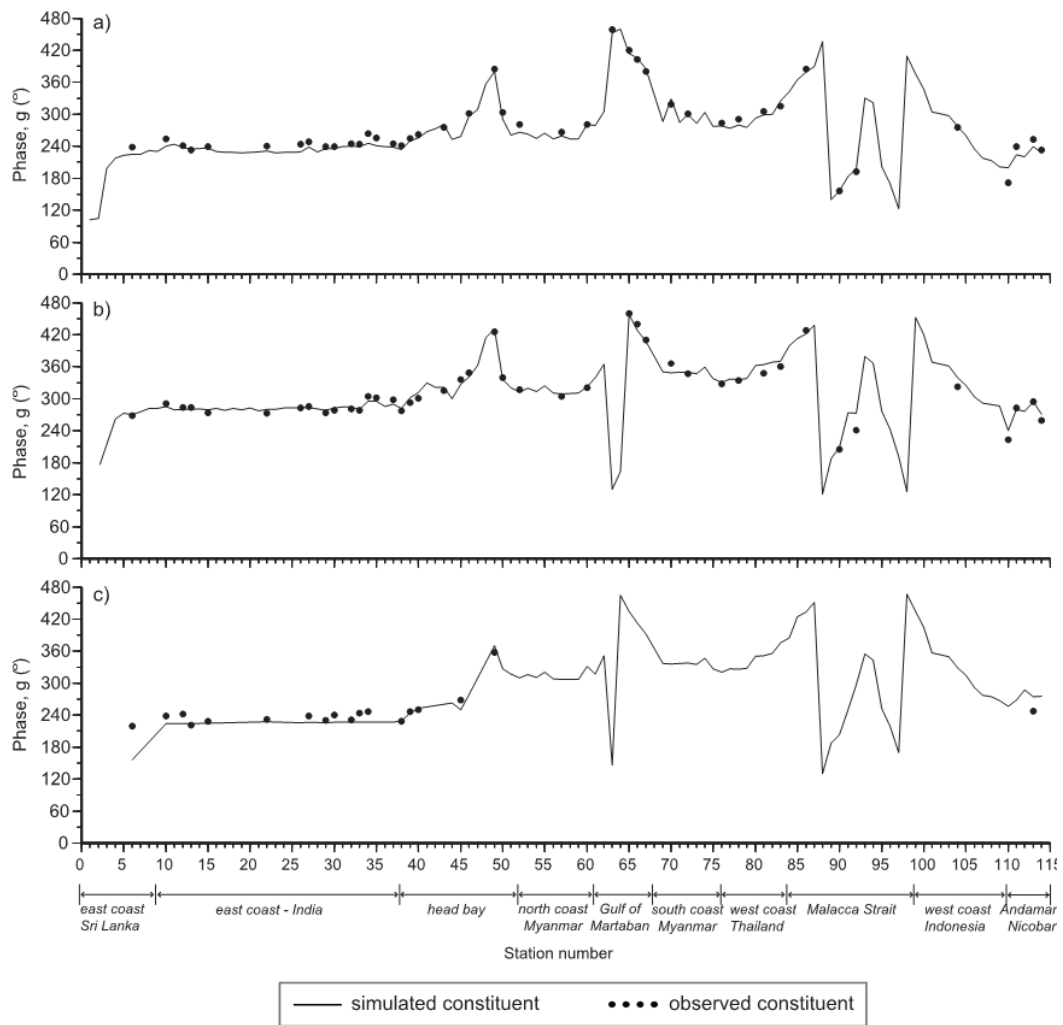
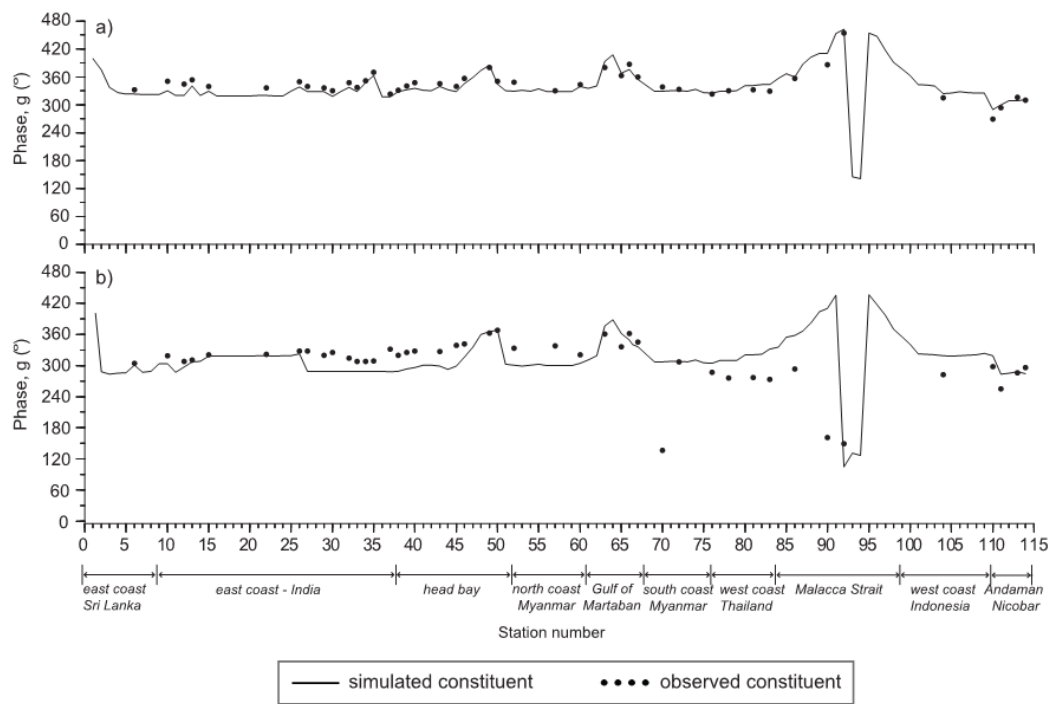


**Figure 4.13** Same as Figure 4.10, but for the phases  $g$  of diurnal constituents, a)  $K_1$  and b)  $O_1$ .



### 4.4.3 Statistical analysis to assess model performance

The performance of the model is demonstrated with scatter plots of model derived and observed amplitudes and phases of the tidal constituents (Figures 4.14 and 4.15, respectively). It is seen that the major semi-diurnal constituents  $M_2$  and  $S_2$  are simulated accurately and except for some outliers, the model derived and observed  $M_2$  and  $S_2$  amplitudes agree favourably with a correlation coefficient of 0.99 and 0.98, respectively. The model derived  $M_2$  amplitudes show some discrepancies at Sagar Roads, Sabang, Galathea Bay and KoHoKya while  $S_2$  amplitudes stand out as outliers at Sabang and Galathea Bay. However, at nearby locations of these stations, the model-derived amplitudes are found to be close to the observed amplitude suggesting the presence of some local phenomena that the model cannot resolve. The amplitudes of diurnal constituent  $O_1$ , being relatively lower than the semi-diurnal constituents, show larger scatter. The scatter plot for the phases of the tidal constituents indicates good agreement between the model derived and observed phases of all constituents (correlation coefficient close to 0.99) except for  $O_1$  which show low correlation of 0.92.

The accuracy of the model results is quantified by estimating mean error (ME) and root mean square error (RMSE) as shown in Equations (4.1) and (4.2) respectively for amplitudes and phases of each of the model derived constituents [Robertson et al., 1998].

$$ME_i = \frac{1}{N} \sum_N e_i \quad (4.1)$$

$$RMSE_i = \left[ \frac{1}{N} \sum_N e_i^2 \right]^{\frac{1}{2}} \quad (4.2)$$

where  $\bar{e}_i$  is the mean error.

In addition, the overall performance of the model is measured by computing the RMS misfit (ORM) as suggested by Matsumoto et al. [2000]:

$$ORM_i = \left[ \frac{1}{N} \sum_N \frac{1}{2} (A_{s,i}^2 + A_{o,i}^2 - 2A_{o,i}A_{s,i} \cos(g_{s,i} - g_{o,i})) \right]^{\frac{1}{2}} \quad (4.3)$$

where,  $A_{s,i}, g_{s,i}$  are the model derived amplitude and phase and  $A_{o,i}, g_{o,i}$  are the observed amplitude and phase, respectively of the  $i^{th}$  constituent.

At majority of stations, the tidal amplitudes of  $M_2, S_2, K_1$  and  $O_1$  derived from the model agree to within 10, 8, 8 and 5 cm respectively of the observed values. The model, on an average, slightly over-estimates the semi-diurnal amplitudes and under-predict the diurnal amplitudes. The largest discrepancies between model results and observations occur in the prediction of  $M_2$  amplitude, as depicted by RMSE, probably due to the outliers seen in Figure 4.14.

The ME computed for the phases of the tidal constituents indicate a phase lag of 9 and 12 minutes for  $M_2$  and  $K_1$  tide, respectively, compared to the observed phases while  $S_2$  and  $O_1$  tides, on an average, appear to arrive earlier by 3 and 7 min, respectively than the observed tide (Table 4.2). The high RMSE for the  $O_1$  phase is assessed to be due to sudden significant change in the phase observed at Sinbyubyn station ( $136^\circ$ ) compared to the neighbouring stations (approximately  $315^\circ$ ) which cannot be resolved by the grid resolution considered in the model. If this station is neglected, the RMSE is found to be approximately  $24.8^\circ$  for  $O_1$  phase.

On the whole, there is a reasonable agreement between the model derived and the observed amplitudes and phases of the semi-diurnal and diurnal constituents with RMSE less than 7 cm and  $9.5^\circ$ . It can be concluded from the RMS misfit (ORM), being less than 9 cm for all the model derived constituents, that despite of the discrepancies between the amplitudes and phases of the model derived and observed constituents at few stations, the model has the capability of reproducing the tides in the area and has sufficient fine grid to capture the near shore tidal variations.

**Figure 4.14** Scatter plots of the model derived and observed amplitudes of the tidal constituents a)  $M_2$ , b)  $S_2$ , c)  $K_1$ , and d)  $O_1$  extracted at 44 stations (locations tabulated in Table 4.1 and shown in Figure 4.7). The stations located in different regions (regions categorized as per Table 4.1) are marked with different symbols.

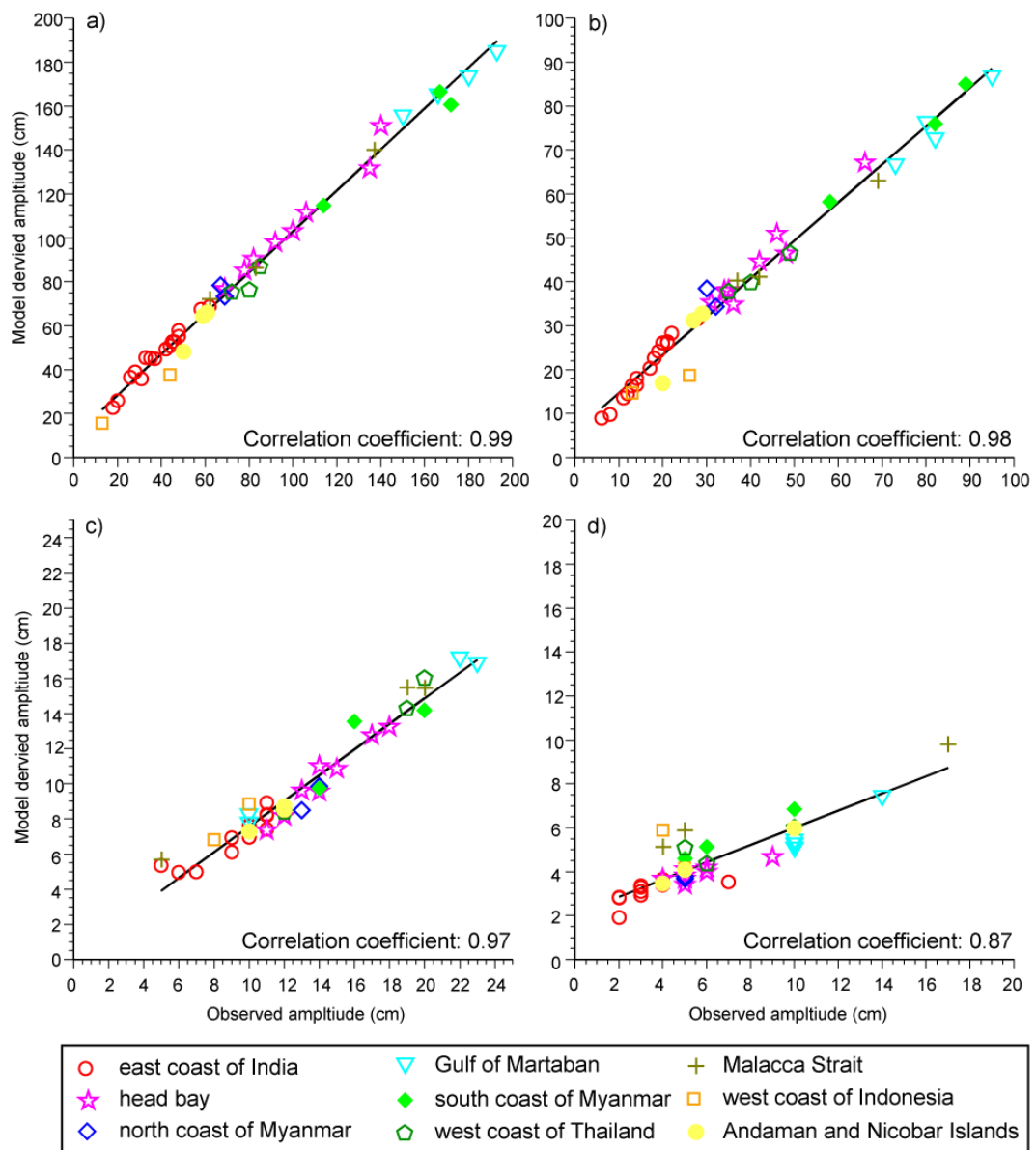




**Figure 4.15** Same as Figure 4.14, but for the phases of the tidal constituents a)  $M_2$ , b)  $S_2$ , c)  $K_1$ , and d)  $O_1$ .

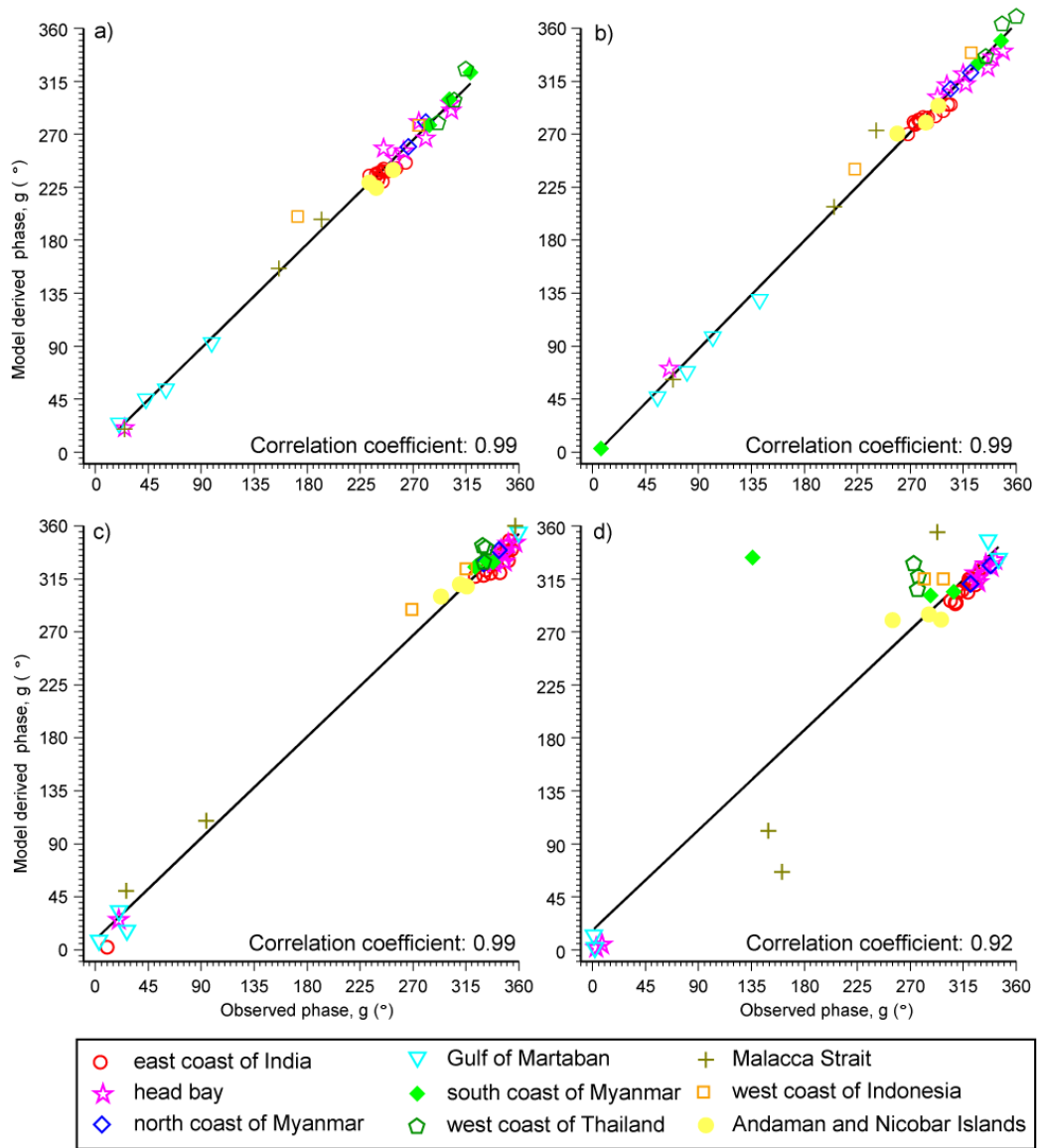


**Table 4.2** Error statistics – Mean Error (ME) and Root Mean Square Error (RMSE) for the model derived amplitudes and phases of the major tidal constituents for the coastal stations. The Root Mean Square misfit (ORM) is also tabulated.

Constituent	ME		RMSE		ORM (cm)
	A (cm)	g (°)	A (cm)	g (°)	
M <sub>2</sub>	4.38	-4.18	7.04	9.43	9.16
S <sub>2</sub>	1.18	1.59	4.44	8.91	5.64
K <sub>1</sub>	-3.16	-3.64	3.45	11.06	2.89
O <sub>1</sub>	-1.45	1.48	2.47	38.53	3.05

#### 4.4.4 Comparison between simulated and predicted tides extracted from Indian Tide Tables

The datum and time zone of tidal elevations extracted at grid points closest to the location of remaining 10 Standard Ports were also adjusted in time and space, as described in Section 4.4.1 and compared against the predicted high and low waters obtained from ITT for the month of August 1981, covering a spring – neap cycle, as shown in Figures 4.16 to 4.19.

The comparison ensures the efficiency of the model in reproducing the observed tidal range and pattern at all stations that could represent the entire modelled coastline. Therefore, the general characteristic of tides along the coast of Bay Bengal can be described using the model results.

**Figure 4.16** Comparison of simulated tidal elevations (cm) (black line) with predicted high and low water levels (circles), obtained from Indian Tide Tables, at a) Trincomalee (along east coast of Sri Lanka), b) Kakinada (along the east coast of India) and c) Port Blair (along the coast of Andaman Islands). The time 00 hours corresponds to 00 hours on August 01, 1981.

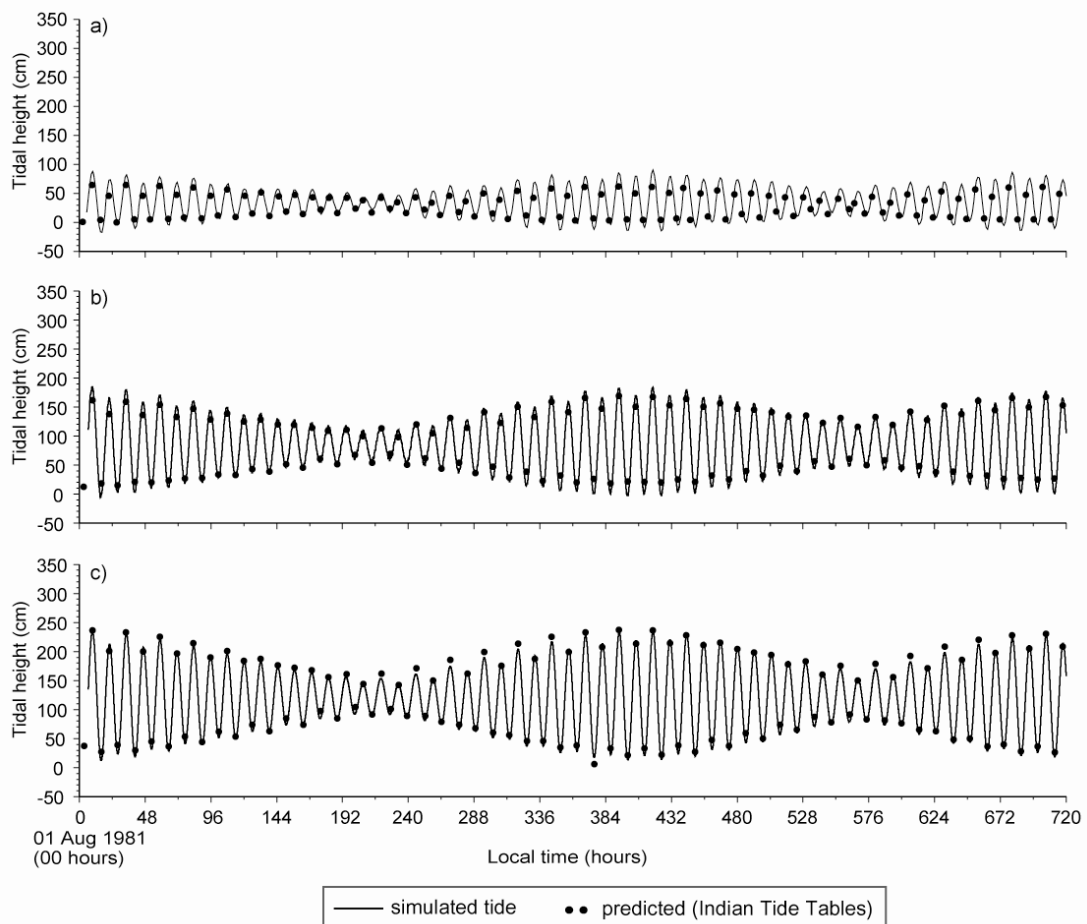


**Figure 4.17** Same as Figure 4.16, but for stations in the head bay, a) Shortt Island and b) Sagar Roads.

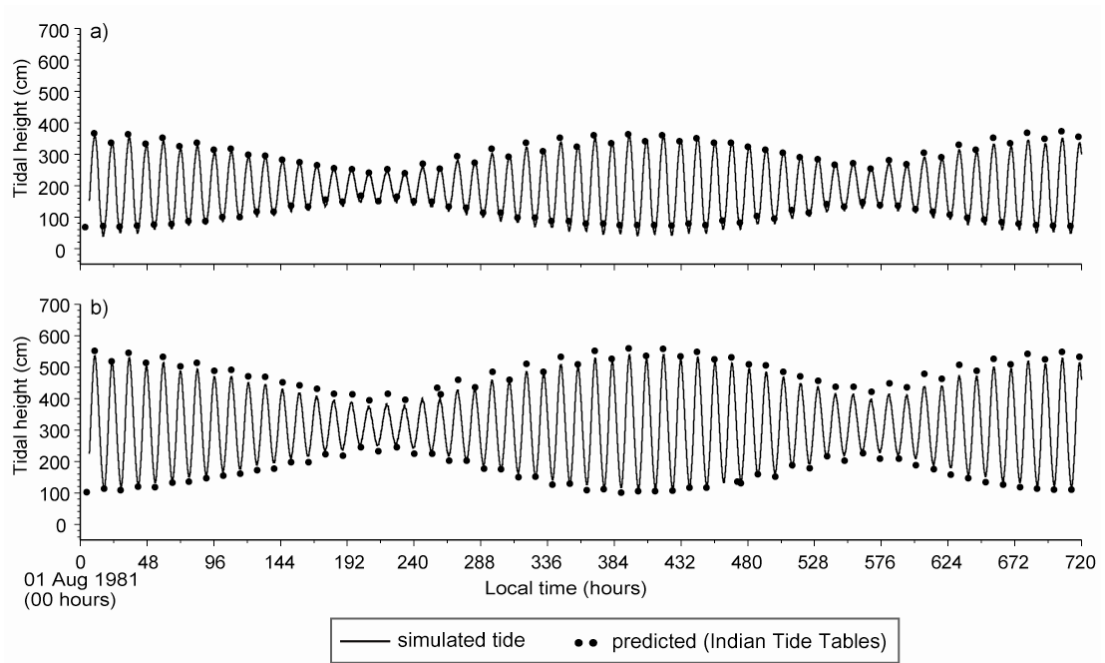


**Figure 4.18** Same as Figure 4.16, but for stations along the northern coast of Myanmar at a) Akyab and for stations in the Gulf of Martaban, b) Amherst and c) Mergui.

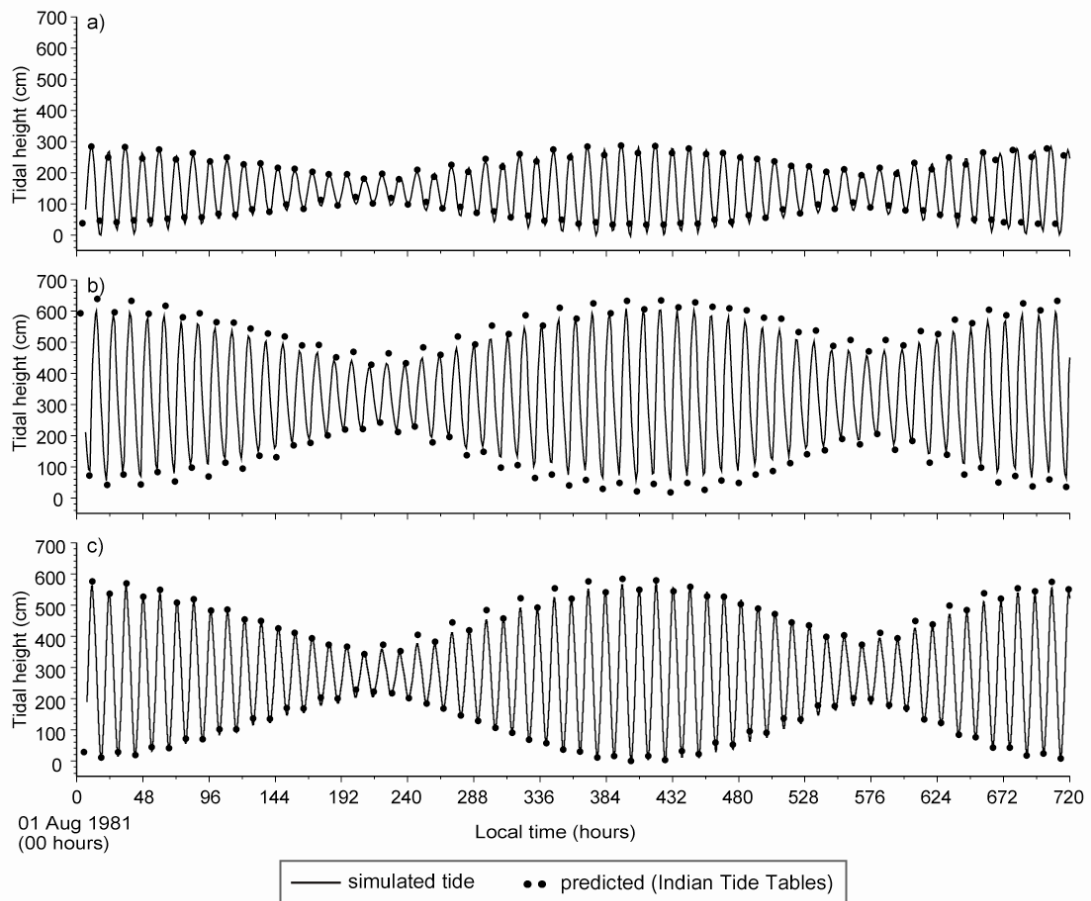
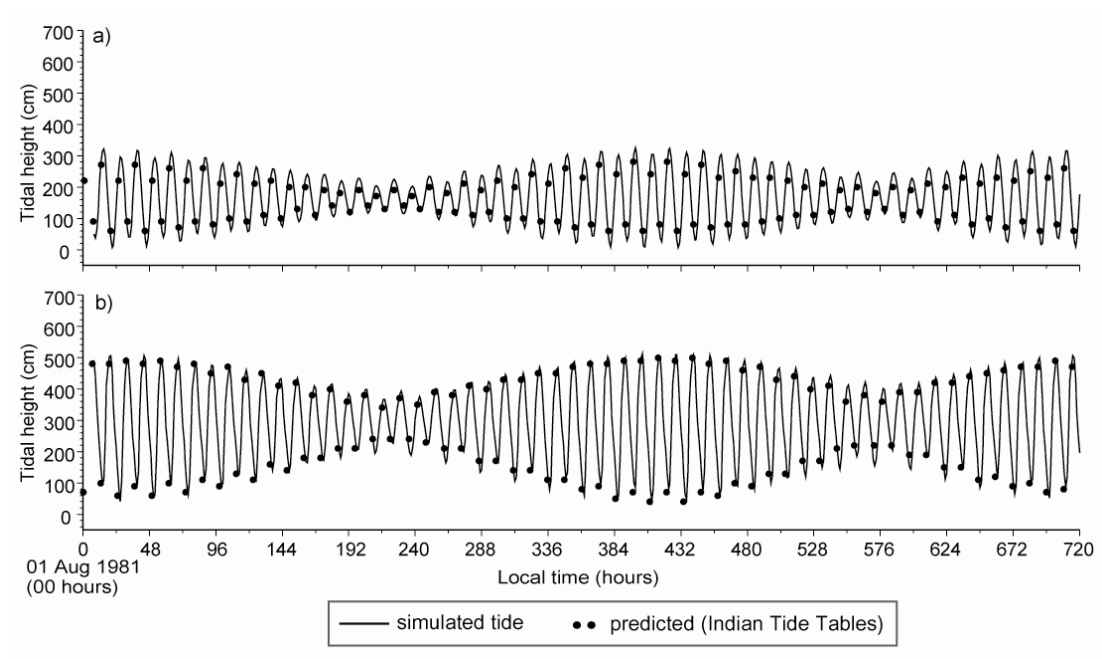


**Figure 4.19** Same as Figure 4.16, but for stations along the west coast of Thailand at (a) Pinang, and b) Pelabuhan Klang.



Approximate tidal ranges calculated from simulated tidal elevations during spring and neap tide at 13 stations are presented in Table 4.3. The tidal range is found to be lowest at Trincomalee in Sri Lanka. Along the coast of India, the tidal range vary significantly with relatively low range of 1.1 m at Chennai and reaching as high as 5.3 m at Sagar Roads, located in the head bay as seen from Table 4.3. It is noted that relatively higher tidal range is found at Mergui, located along the coast of Myanmar as compared to the tidal ranges at stations in the head bay. Table 4.3 shows that the highest tidal range (approximately 6.2 m) is observed at Amherst, which is located in the Gulf of Martaban.

**Table 4.3** The spring and neap tidal range obtained from the simulated composite tidal elevation time series data extracted at the 13 Standard Ports (name and location tabulated in bold letters in Table 4.1 and shown as solid circles in Figure 4.7).

Station No	Station Name	Spring tidal range	Neap tidal range
6	Trincomalee	0.6	0.1
15	Chennai	1.1	0.2
27	Kakinada	1.5	0.3
29	Visakhapatnam	1.6	0.3
38	Paradip	2.0	0.4
40	Shortt Island	3.0	0.7
43	Sagar Roads	5.3	1.5
113	Port Blair	2.4	0.4
52	Akyab	2.5	0.6
65	Amherst	6.2	0.4
72	Mergui	5.8	1.1
86	Pinang	2.2	0.3
90	Pelabuhan Klang	4.7	1.0

## 4.5 Simulation of tidal constituents

The tidal elevations applied at the open boundaries of the tidal model was modified, as described in this section, to simulate separately each of the major semi-diurnal ( $M_2$ ,  $S_2$  and  $N_2$ ) and diurnal ( $K_1$  and  $O_1$ ) tidal constituents.

A time series of tidal elevation was constructed for a period of 40 days by using the amplitude and phase of  $M_2$  tide, extracted from FES2004 dataset at selected grid points. The  $M_2$  tidal time series was interpolated to each grid point along the open boundaries of the tidal model. The simulated  $M_2$  tidal elevation was stored at hourly intervals starting from the 10<sup>th</sup> day at each grid point of the model domain. The amplitudes and phases, computed from the simulated elevations of  $M_2$  tide at each grid point of the model domain, were used to generate co-range (contour maps showing lines of equal amplitudes) and co-tidal charts (contour maps showing lines of equal phases), respectively. Similar procedure was followed for the simulation of  $S_2$ ,  $N_2$ ,  $K_1$  and  $O_1$ .

## 4.6 Co-range and co-tidal charts

This section describes the general characteristics of the tidal constituents in the Bay of Bengal and the characteristic features identified from the co-range and co-tidal charts in the shallow regions of the Bay of Bengal.

### 4.6.1 General features

The co-range and co-tidal charts for the semi-diurnal constituents  $M_2$ ,  $S_2$  and  $N_2$  are presented in Figures 4.20, 4.21, and 4.22, respectively. The charts show a degenerate amphidromic system along the south eastern coast of Sri Lanka.

The  $M_2$  amplitude tends to increase northward and north-eastward while entering the head bay and the Gulf of Martaban (Figure 4.20a). The distribution of  $M_2$  tide in the Bay is affected by the presence of Andaman Island. In the central Bay, the  $M_2$  tide propagates north-westward from the amphidromic point into the central bay and then attains a northward propagation in the head bay. In the



Andaman Sea, tide progresses north-eastward and enters into the Gulf of Martaban while in Malacca Strait, tide propagate southward (Figure 4.20b).

The amplitudes of the  $S_2$  tide is about half of the  $M_2$  tide and their variations in the Bay are similar to those of  $M_2$  tide (Figure 4.21a). The  $S_2$  tide propagates northward from the amphidromic point in the central Bay while in the Andaman Sea and Malacca Strait, similar to the  $M_2$  tide,  $S_2$  propagates north-eastward and southward, respectively (Figure 4.21b).

The amplitude of  $N_2$  (Figure 4.22a) is low compared to the amplitudes of the other two semi-diurnal constituents. Though variations in  $N_2$  amplitude in the central bay are less, local maxima occur in the head bay and in the Gulf of Martaban.

The co-range and co-tidal charts for  $K_1$  (Figure 4.23) depict only small variations in the amplitude and phase across the Bay. The amphidromic system identified along the south eastern coast of Sri Lanka from the co-range and co-tidal charts of the semi-diurnal tides is found to be located along the open boundary for  $K_1$  tide. The propagation of the  $K_1$  tide, similar to  $M_2$ , is towards north-west and south-east in the central bay and Malacca Strait, respectively. The  $K_1$  amplitude is found to be highest in the Malacca Strait unlike the semi-diurnal tides ( $M_2$ ,  $S_2$  and  $N_2$ ), which have highest amplitudes in the Gulf of Martaban. These localized features are described in detail in the next section.

The co-range charts (Figure 4.24a) of  $O_1$  show a gradual increase in amplitude towards the head bay, but the amplitudes are very small, the maximum amplitude being 10 cm in the Malacca Strait. The degenerate amphidromic system in the  $O_1$  chart is located at the southern tip of Sri Lanka, around which tide progresses in the counter-clockwise direction. The  $O_1$  tide propagates northward (Figure 4.24b) in the central western bay while in the Andaman Sea and inside the Malacca Strait, the propagation of the  $O_1$  tide is similar to that of  $K_1$  but the amplitudes are lower.

**Figure 4.20** Distribution of amplitudes and phases of  $M_2$  tide in the Bay of Bengal simulated using the tidal model showing a) co-range lines and b) co-tidal lines. Amplitudes are given in centimetres and phase 'G' is given in degrees. The area marked as Detail 1, Detail 2 and Detail 3 are shown in Figure 4.26, Figure 4.28, and Figure 4.30, respectively.

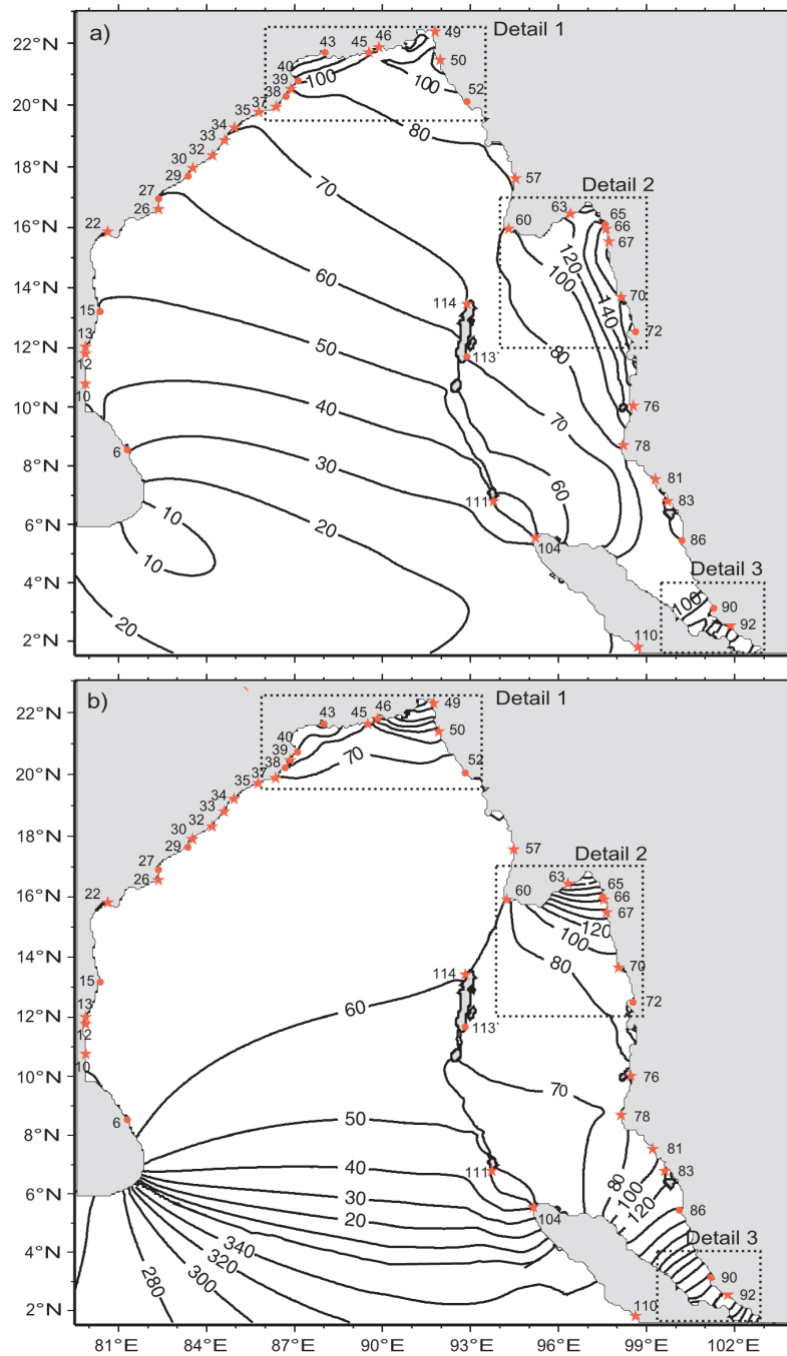


**Figure 4.21** Same as Figure 4.20, but for  $S_2$  tide. The area marked as Detail 1, Detail 2 and Detail 3 is shown in Figure 4.27, Figure 4.29, and Figure 4.31, respectively.

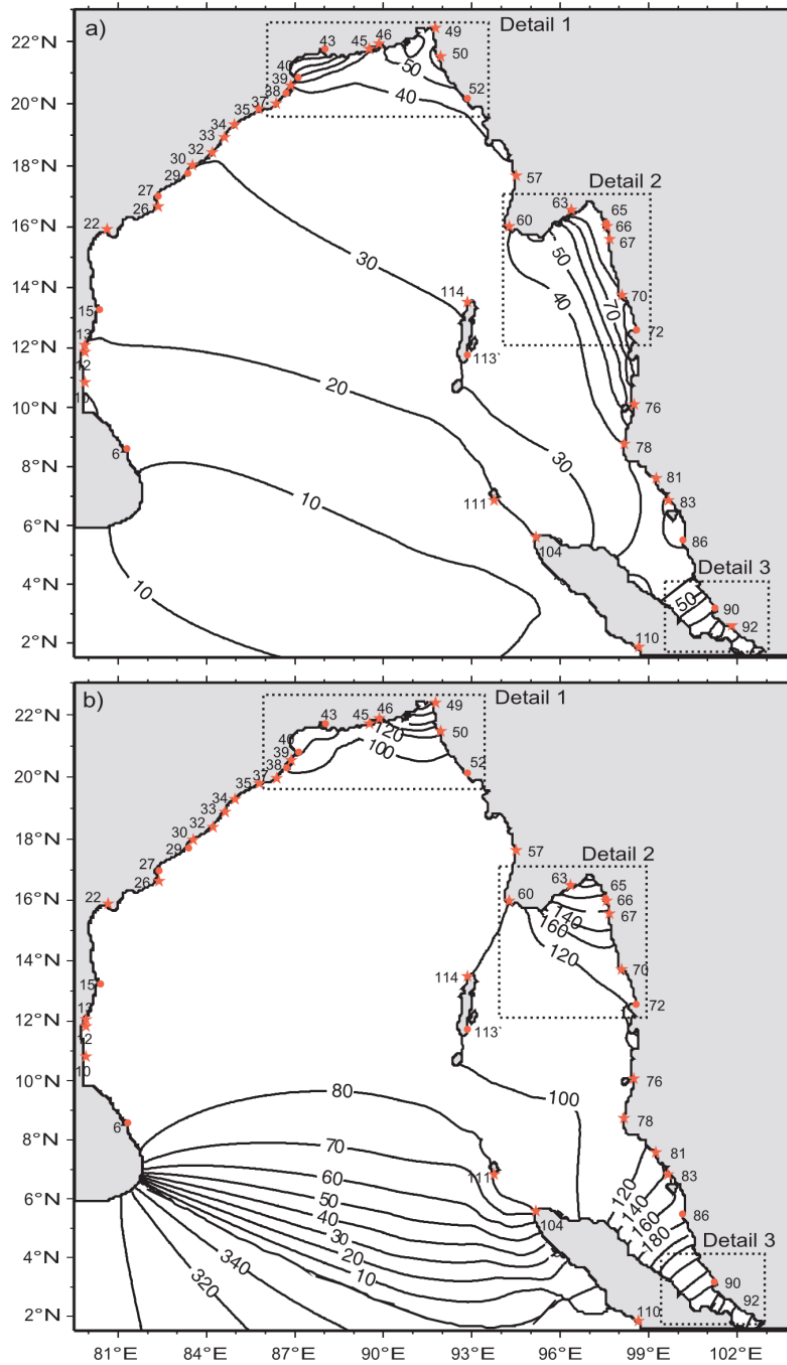
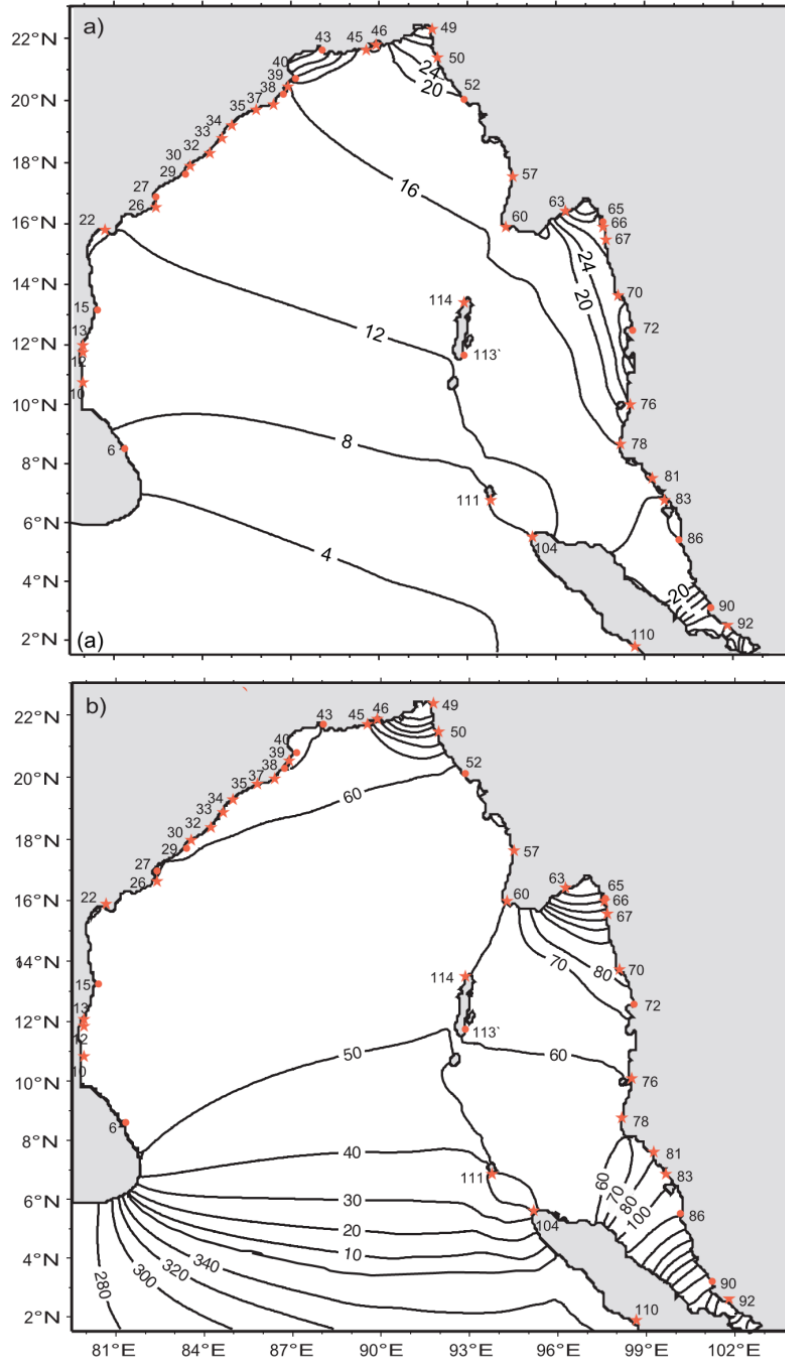


Figure 4.22 Same as Figure 4.20, but for  $N_2$  tide.



**Figure 4.23** Same as Figure 4.20, but for  $K_1$  tide. The area marked as Detail 3 is shown in Figure 4.32.

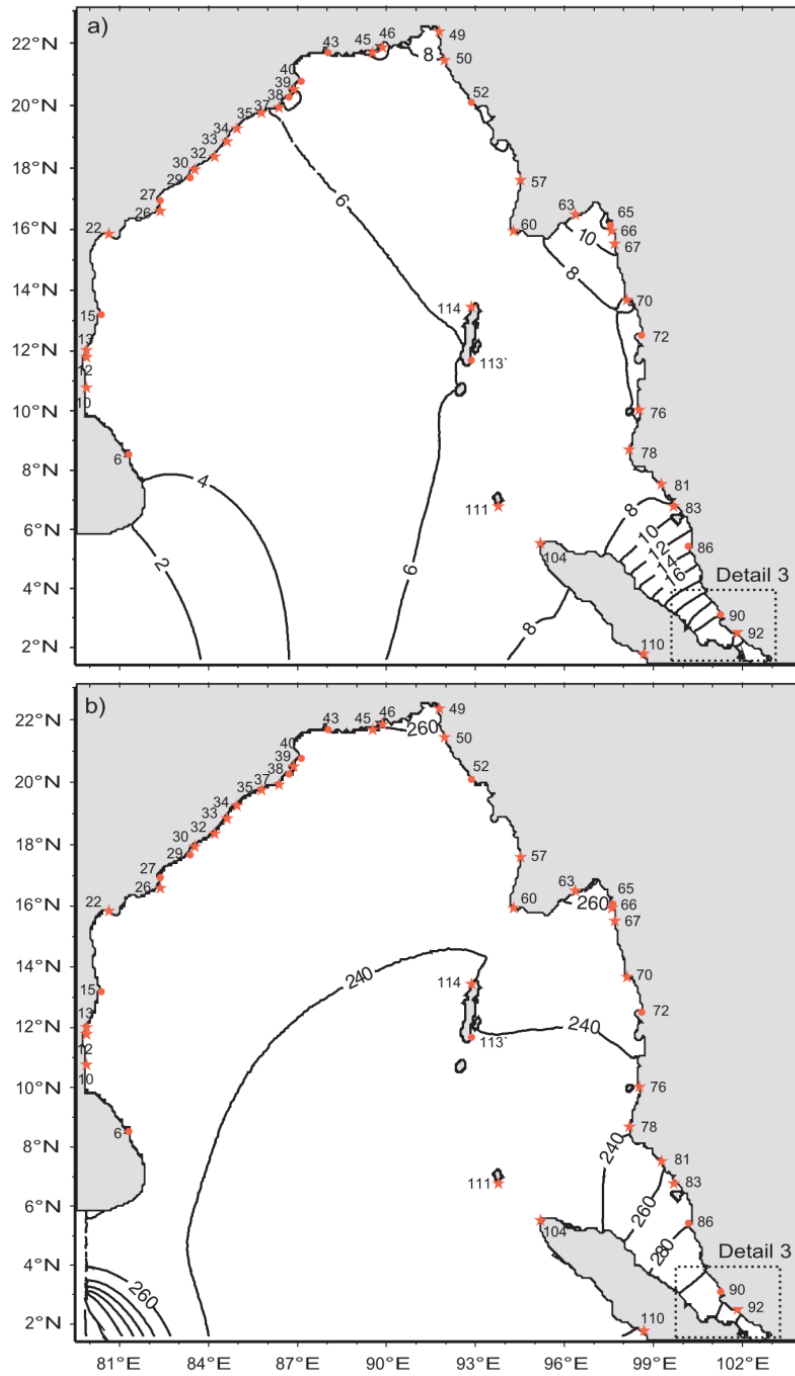
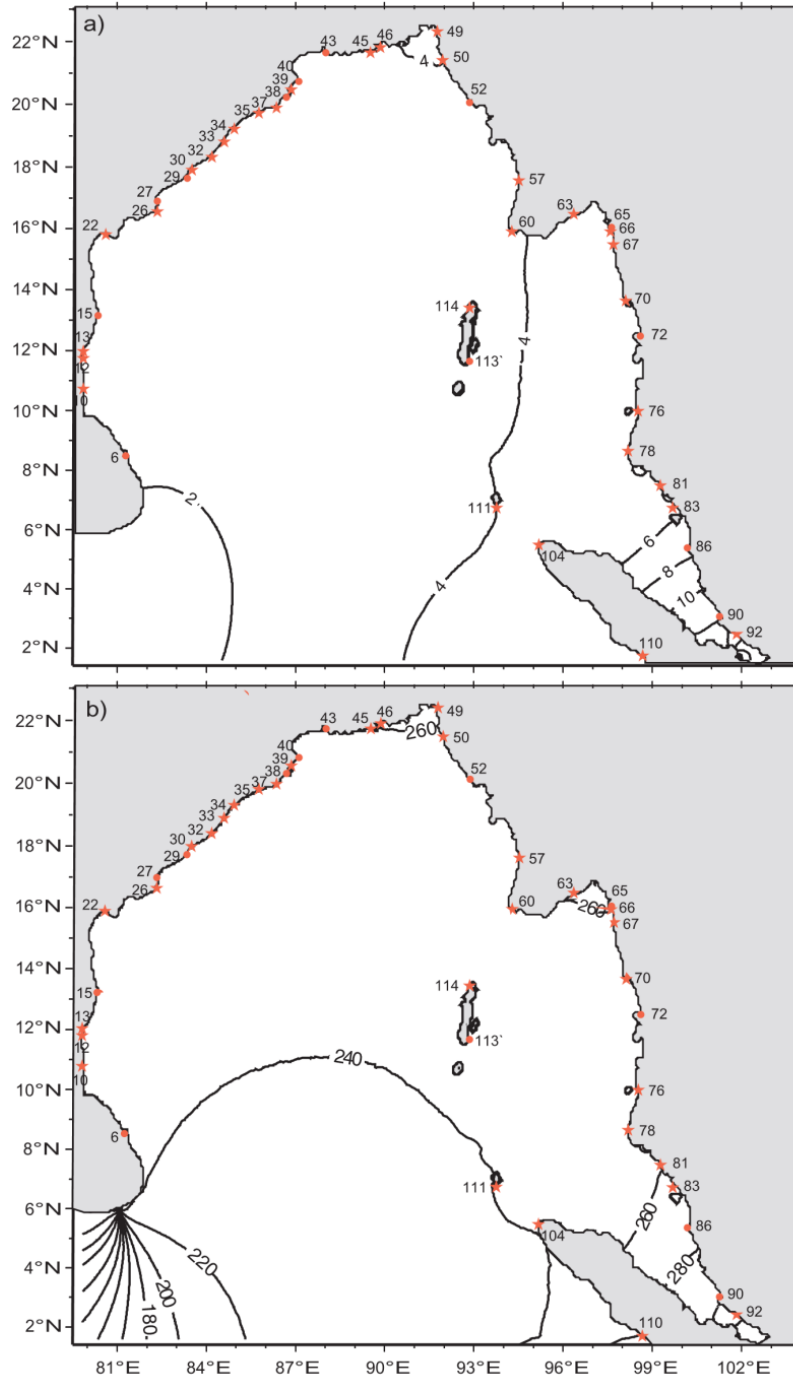


Figure 4.24 Same as Figure 4.20, but for  $O_1$  tide.



## 4.6.2 Characteristic features

Some characteristic features are observed in the distribution of the amplitudes and phases of tidal constituents in the shallow regions of Bay of Bengal such as the head bay, Gulf of Martaban and Malacca Strait. For semi-diurnal constituents, the detailed view of the co-tidal and co-range charts in these regions is shown in Figures 4.26 to 4.31 and for diurnal constituent, the detailed view is shown only for the Malacca Strait in Figure 4.32.

### Head Bay

The amplitudes of the semi-diurnal tides in the head bay are found to be doubled in the head bay. The essential feature that could significantly contribute to the increase in the amplitudes of semi-diurnal tides in the head bay is its wide continental shelf, as analyzed in below section.

The effect of continental shelf is studied using the theory formulated by Clarke and Battisti [1981], referred to as CB theory in the text. They showed that semi-diurnal tides amplify on wide shelves in non-polar latitudes while the diurnal tides do not. They related the amplification of semi-diurnal tides to the proximity between shelf width and a parameter called shelf scale parameter (defined as  $SP = \frac{g\alpha}{\omega^2 - f^2}$ , where  $\alpha$  is the bottom slope,  $f$  is the Coriolis parameter (described in Section 2.2) and  $\omega$  is the angular frequency of the tidal constituent ( $\omega = 2\pi/T$ ,  $T$  being the constituent period given in Table 1.1).

Murty and Henry [1983] also applied the CB theory at some stations in the head bay to study the effect of continental shelf width in the head bay. But, in the present study, we applied the theory to other regions along the western and eastern coast of Bay. We estimated the amplification factor (AF, the ratio of tidal amplitude at the coastal station to that at the shelf break) and the shelf scale parameter (SP) for  $M_2$ ,  $S_2$ ,  $N_2$  and  $K_1$  in order to investigate the effect of continental shelf width. Though SP and AF were extracted for all stations shown in Figure 4.7, except for the stations located far inside the head bay, Gulf of Martaban and Malacca Strait, Table 4.4 documents the values only for Standard

and Secondary Ports. Figure 4.25 shows the impact of the continental shelf width on the variability of AF of  $M_2$ ,  $S_2$ ,  $N_2$  and  $K_1$ .

Amplification of semi-diurnal tides is not observed along the east coast of India; where the continental shelf is narrow (width less than 100 km). But in the head bay, continental shelf widens (approximately 200 km) and therefore semi-diurnal tides amplify in the region. For instance, the  $M_2$ ,  $S_2$  and  $N_2$  tides attain an AF of 1.9, 2.5 and 1.9, respectively at Sagar Roads (Table 4.4), and an AF of 1.8, 2.3, and 1.7, respectively at Chandipur, which are located on western part of head bay. The continental shelf at Sagar Roads and Chandipur is as wide as 195 and 160 km, respectively which are relatively closer to the value of SP as seen from Table 4.4. The diurnal tide  $K_1$  amplifies only marginally in the western part of the head bay (AF=1.1 at Sagar Roads). This is in agreement to CB theory. However at the locations of Pussur River and Tiger Point, the amplitudes of semi-diurnal tides are not relatively high (for  $M_2$ , AF = 1.2 at both stations), which could be due to relatively narrow shelf (approximately 100 km), as seen from Table 4.4.

In the eastern head bay, the amplification of semi-diurnal tides is relatively less (AF at Chittagong is 1.5, 1.6 and 1.9, respectively), but in this region the diurnal tide  $K_1$  is observed to amplify equally as that of semi-diurnal tides as indicated by AF of 1.5 at Chittagong. Therefore, in addition to the wide continental shelf (as assessed from Figure 4.8), the geometrical configuration of the coastline in the north-eastern head bay could also be responsible for the amplification of both semi-diurnal and diurnal tides in the region.

The detailed examination of the  $M_2$  and  $S_2$  charts (Figures 4.26b and 4.27b, respectively) revealed the presence of a degenerate amphidromic point near to Pussur Station. Another degenerate amphidromic point is identified at the north eastern end of head bay (Figures 4.26c and 4.27c).

### **Gulf of Martaban**

The co-range charts of semi-diurnal constituents (Figures 4.20, 4.21, and 4.22) the highest amplification of semi-diurnal tides ( $M_2$ ,  $S_2$ , and  $N_2$ ) is found to be in the Gulf of Martaban; the AF being 2.4, 2.8, and 2.6 at Amherst (Table 4.4). The



amplification of  $M_2$  and  $S_2$  are found to be higher (by 23% and 29%, respectively) along the eastern coast of Gulf of Martaban as compared to the western coast. The diurnal tide  $K_1$  amplifies significantly (AF=1.7) in the Gulf of Martaban. The converging effect of the funnel shaped gulf, shallow bathymetry and the wide continental shelf could contribute to the amplification, consequently producing very high tidal amplitudes in the area.

### **Southern part of Myanmar coast**

One of the interesting features observed in the distribution of semi-diurnal co-range and co-tidal charts is the amplification of  $M_2$ ,  $S_2$ , and  $N_2$  along the southern coast of Myanmar, with amplitudes increasing southward and attaining relatively higher values near Sinbyubyin (AF = 1.8, 1.9 and 1.4, respectively) and Mergui (AF = 2.0, 2.2 and 1.6, respectively) than those at Akyab and Gya Bay (AF = 1.1 and 1.0 at 2 stations, respectively for  $M_2$ ,  $S_2$ , and  $N_2$ ), which are located on the northern Myanmar coast. The coastline of Myanmar is characterized by a wide continental shelf, especially at the southern coast, where the shelf is as wide as 220 km. It is evident from Table 4.4 that the shelf scale parameter (SP), estimated for stations along southern Myanmar coast (Stations 68 to 72), is in close proximity to the shelf width, which signifies the amplification of semi-diurnal tides. The diurnal tide  $K_1$  amplifies only marginally at these stations in compliance with the theory of CB theory. Figure 4.25 also depicts that the variations in the amplitudes of  $K_1$  tide is very small with the variation in shelf width along the coast of Bay of Bengal.

**Table 4.4** The shelf scale parameter (SP) and the amplification factor (AF - ratio of amplitude at the coastal station to that at the shelf break) estimated for the tidal constituents  $M_2$ ,  $S_2$ ,  $N_2$  and  $K_1$  at stations corresponding to the Standard and Secondary Ports. The shelf width estimated at each of the stations, excluding the stations located inside the Gulf of Martaban and Malacca Strait, is also listed.

St No	Station Name	Shelf width (km)	$M_2$		$S_2$		$N_2$		$K_1$	
			SP	AF	SP	AF	SP	AF	SP	AF
6	Trincomalee	32	1565	1.04	1458	1.04	1627	1.01	6222	1.04
10	Nagapattinam	84	1346	1.03	1253	1.03	1400	1.01	5584	1.03
11	Porto Nova	29	1500	0.99	1400	0.98	1500	0.99	6000	0.99
12	Cudallore	57	1394	1.00	1298	1.00	1451	1.00	5925	1.00
13	Pondicherry	71	1473	1.00	1371	1.00	1533	1.00	6300	1.00
15	Chennai	32	1830	1.01	1701	1.01	1905	1.00	8086	1.00
16	Pulicat	30	2470	1.01	2300	1.01	2576	1.00	11020	1.00
18	Gudur	40	2730	1.01	2539	1.03	2845	1.00	12432	1.00
19	Nellore	20	2000	1.01	585	1.02	5900	1.00	26221	1.00
20	Kavali	40	2810	1.01	2610	0.93	2928	1.00	13168	0.99
22	Surya Lanka	37	450	1.13	418	1.14	1238	1.07	2186	1.01
24	Machilipatnam	100	1192	1.02	1106	1.02	1242	1.03	5871	0.98
26	Sacromental	30	2000	0.99	2000	0.99	652	1.00	20591	0.99
27	Kakinad	50	1813	1.02	1681	1.02	1890	1.00	9231	1.02
29	Visakhapatnam	49	1153	1.00	1069	1.00	1203	1.00	6093	1.00
30	Bhimunipatnam	58	1313	1.01	1216	1.01	1370	1.00	7027	1.01
32	Kalingaptnam	44	1325	1.00	1227	1.00	1382	1.00	7253	0.99
33	Baruva	55	1046	1.01	969	1.01	1092	1.00	5896	1.00
34	Gopalpur	83	1271	1.01	1176	1.01	1327	1.00	7345	1.00
35	Chilka Mouth	92	1049	0.99	971	0.99	1096	0.99	6267	1.00
36	Puri	85	1517	0.99	1403	0.99	1584	0.99	9113	0.99
37	Devi River	34	1887	0.99	1745	0.99	1971	0.98	11398	1.00
38	Paradip	41	569	0.93	526	0.90	594	0.88	3516	0.90

**Table 4.4** Continued

St No	Station Name	Shelf width	M <sub>2</sub>		S <sub>2</sub>		N <sub>2</sub>		K <sub>1</sub>	
			SP	AF	SP	AF	SP	AF	SP	AF
39	False Point	65	446	1.06	412	1.09	466	1.08	2809	1.01
40	Shortt Island	104	445	1.21	411	1.31	465	1.28	2858	1.05
41	Chandipur	160	840	1.78	776	2.33	878	1.72	5658	1.07
43	Sagar Roads	195	614	1.93	567	2.53	642	1.88	4257	1.13
45	Pussur River	100	677	1.25	625	1.27	708	1.04	4690	0.93
46	Tiger Point	110	657	1.21	606	1.28	687	0.99	4619	0.94
49	Chittagong	-	254	1.54	235	1.65	-	1.89	-	1.57
50	Cox Bazaar	-	232	1.32	214	1.70	-	2.00	-	1.19
52	Akyab	81	434	1.11	401	1.13	453	1.09	2651	0.99
57	Gya bay	56	2000	1.02	2000	1.02	2403	1.00	12117	1.00
60	Basien River	185	796	1.08	739	1.07	581	1.12	3880	1.10
63	Elephant	-	-	1.95	-	2.13	-	2.57	-	1.45
65	Amherst	-	-	2.41	-	2.71	-	2.21	-	1.64
66	Double Island	-	-	2.25	-	2.76	-	2.37	-	1.70
68	Bentick Sound	-	-	2.33	-	2.70	-	2.13	-	1.61
70	Sinbyubyin	204	509	1.76	473	1.85	530	1.38	2284	1.10
72	Mergui	220	386	2.00	359	2.25	402	1.63	1674	1.10
76	Pulua basin	145	711	1.51	662	1.56	739	1.32	2903	1.01
78	Klong	88	639	1.10	596	1.10	665	1.03	2547	1.01
81	KoHyaKya	157	303	1.34	282	1.41	315	1.12	1184	1.03
83	Pulua Lela	145	316	1.60	294	1.86	328	1.43	1222	1.24
86	Pinang	-	-	1.68	-	1.94	-	1.40	-	1.57
90	Pelabuhan Kl.	-	-	2.40	-	2.45	-	1.68	-	2.39
110	Sibolga	-	-	1.11	-	1.11	-	1.00	-	1.01

**Figure 4.25** The amplification factor (AF) of  $M_2$ ,  $S_2$ ,  $N_2$  and  $K_1$  tide plotted against the shelf width. The stations far inside the head bay, Gulf of Martaban and Malacca Strait have been excluded.

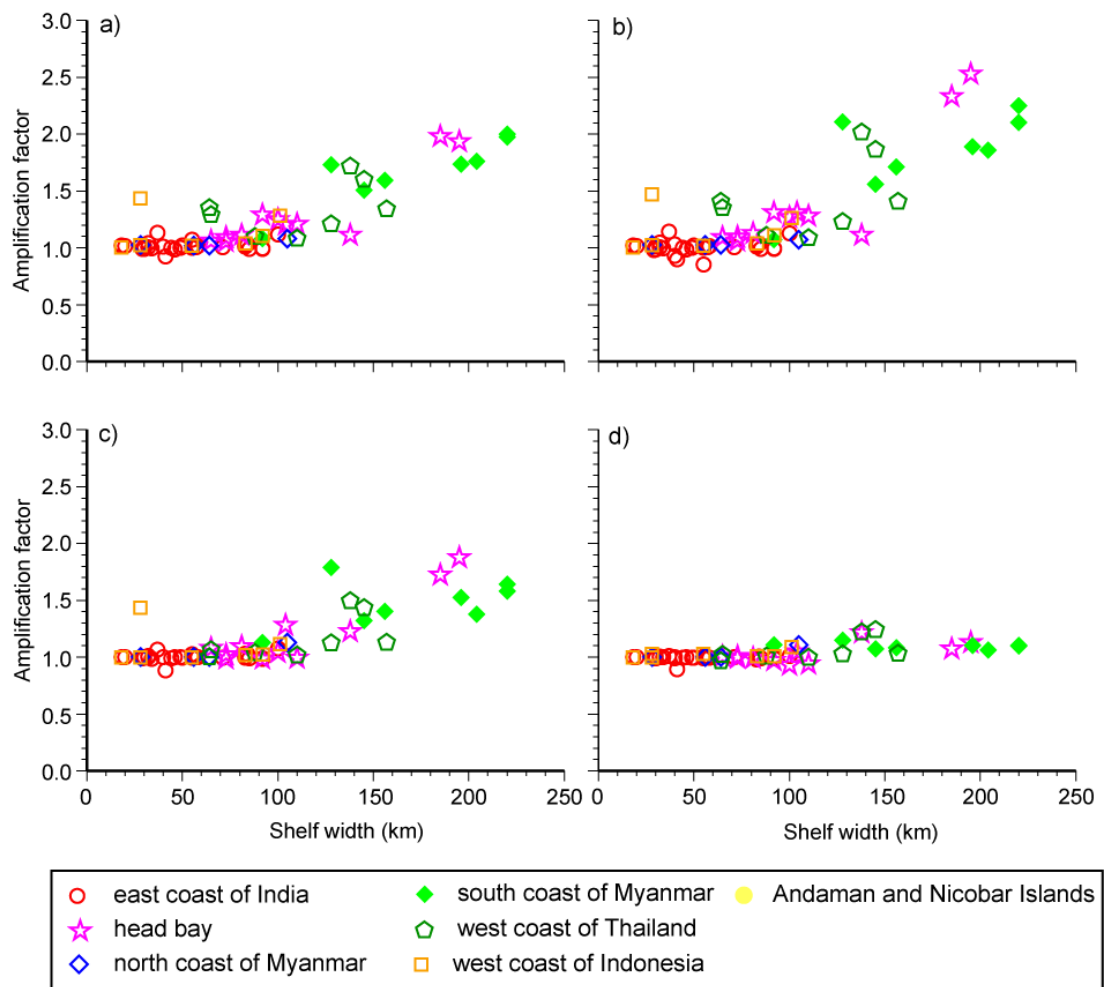


**Figure 4.26** Detailed view of co-range and co-tidal lines of  $M_2$  tide in the a) head bay, showing the degenerate amphidromic points b) along the western and c) north-eastern coast of Bangladesh.

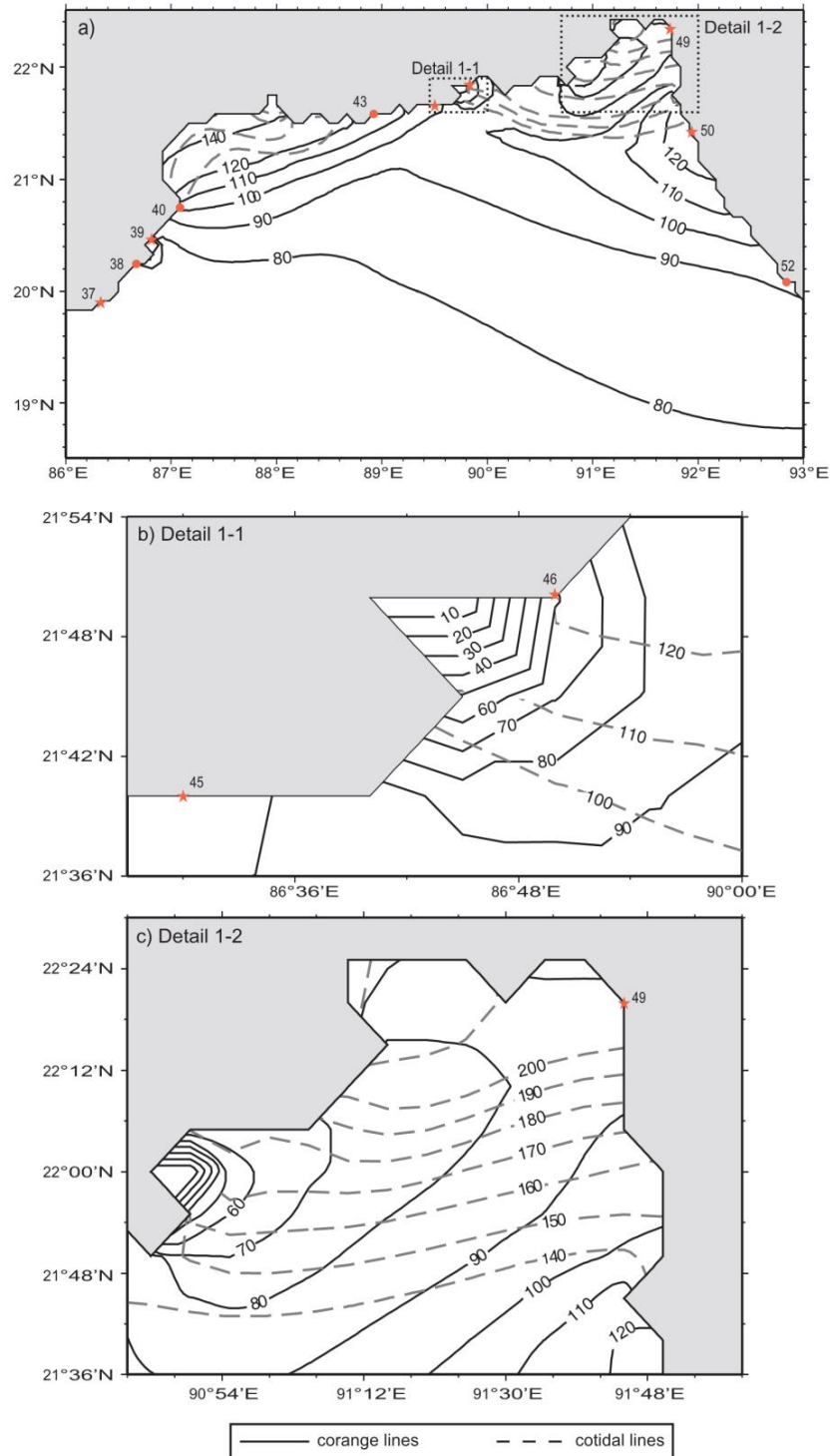


**Figure 4.27** Detailed view of co-range and co-tidal lines of  $S_2$  tide in the a) head bay, showing the degenerate amphidromic points b) along the western and c) north-eastern coast of Bangladesh..

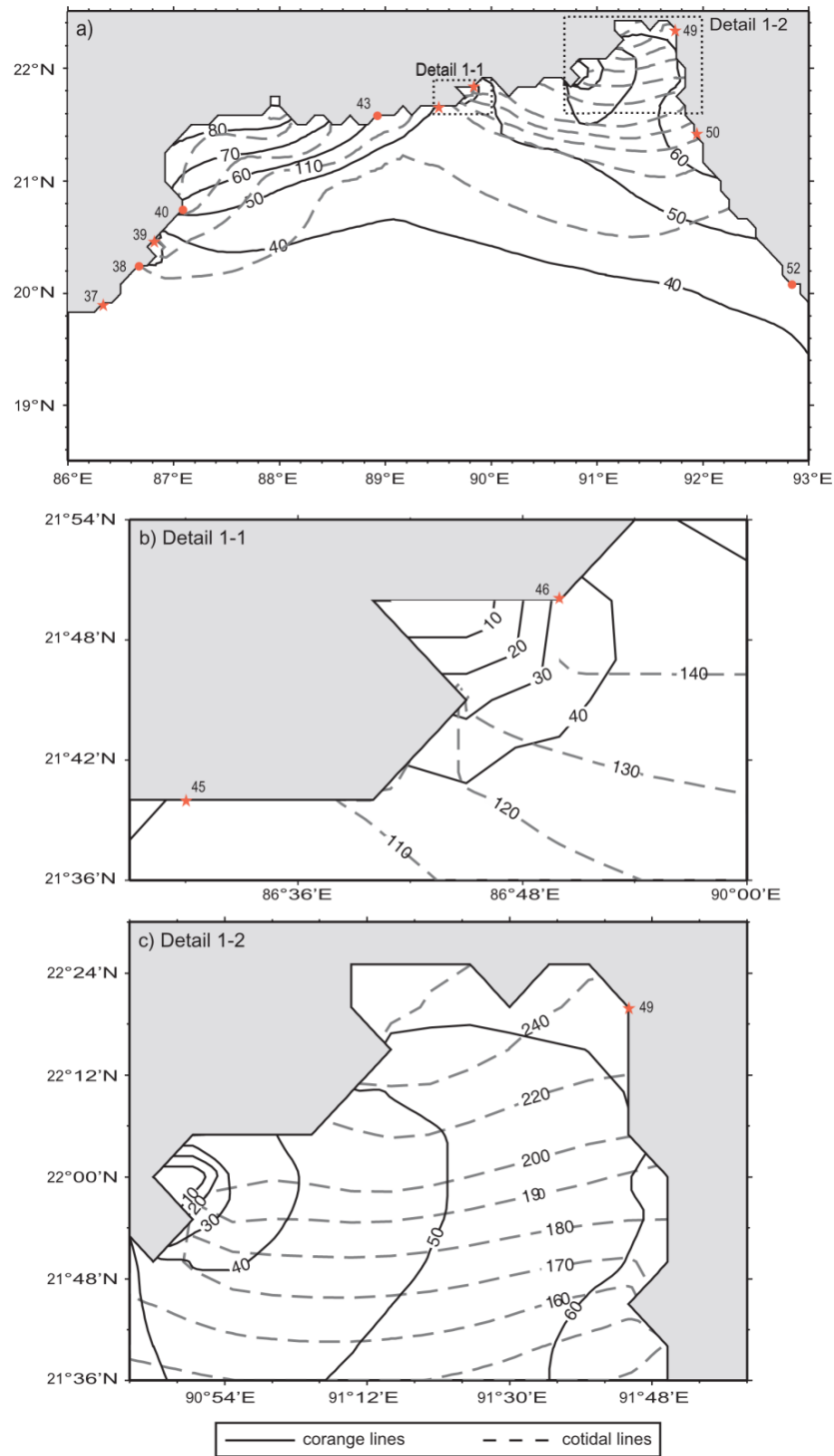


**Figure 4.28** Detailed view of  $M_2$  tidal chart showing the co-range and co-tidal lines for the Gulf of Martaban and along the southern coast of Myanmar.

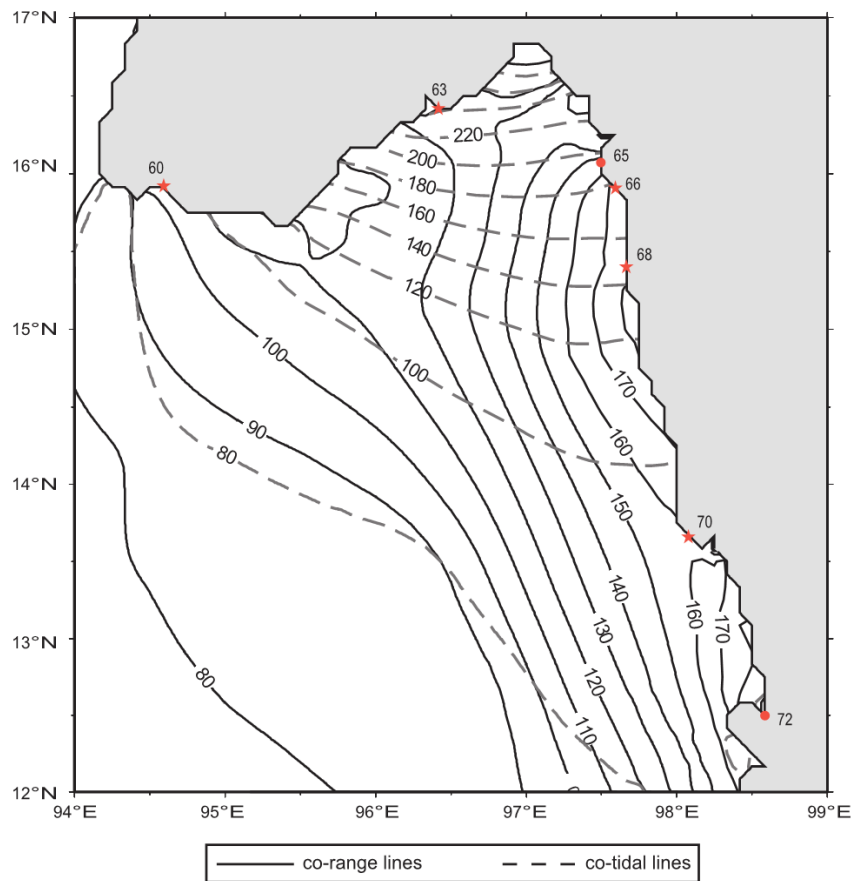
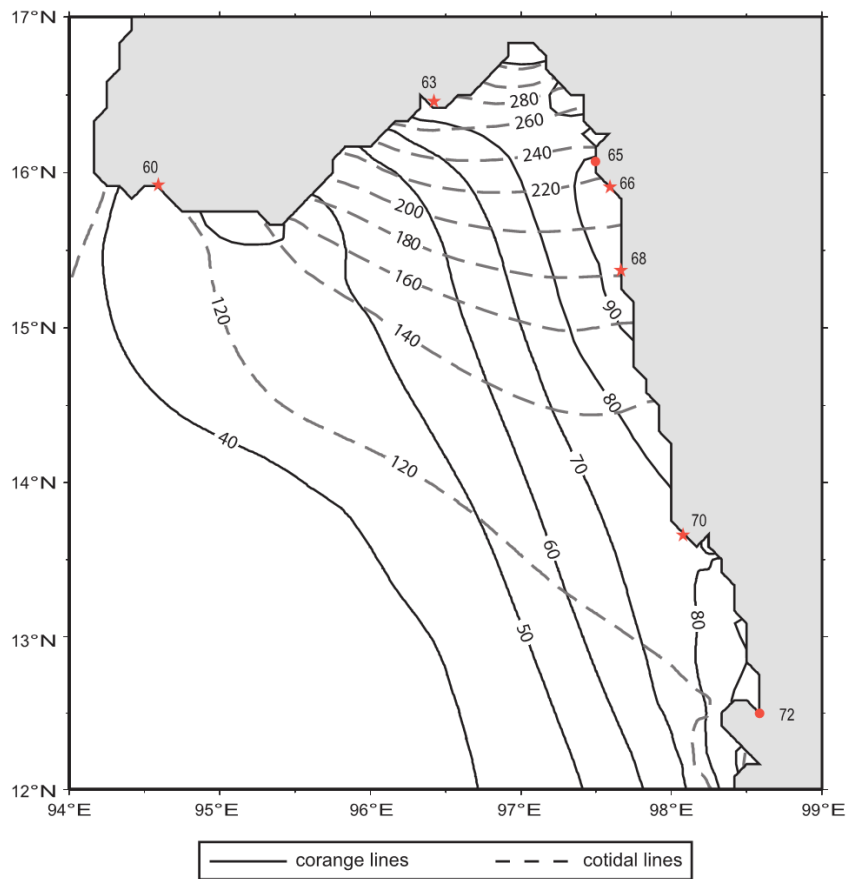


Figure 4.29 Same as Figure 4.28, but for  $S_2$  tide.





### Malacca Strait

The semi-diurnal tides ( $M_2$ ,  $S_2$ ,  $N_2$ ) while entering the Malacca Strait from the northern end show an increase in amplitude towards the southern region with maximum amplitude obtained at about  $2.5^\circ\text{N}$  (i.e. at Pelabuhan Klang, the amplitudes are as high as 130, 60 and 30 cm, respectively).

While analysing the co-range and co-tidal charts for the diurnal tide  $K_1$  (Figure 4.32), we found that along the coast of Bay of Bengal,  $K_1$  attains maximum amplitudes (approximately 20 cm at Pelabuhan Klang) in the Malacca Strait. Even the amplitudes of  $O_1$  tide increases in the Malacca Strait (Figure 4.24), attaining a significant value of 12 cm at Pelabuhan Klang. It is probably the funnel shaped geometrical configuration and shallow bathymetry (depths of average 50 m) of the Malacca Strait, which are favourable for the increase in amplitudes of both semi-diurnal and diurnal tides.

However, the amplitudes of the semi-diurnal and diurnal tides are found to decrease south of  $2.5^\circ\text{N}$ . The amplitude of  $M_2$  tide decreases from  $2.5^\circ\text{N}$  (120 cm) to  $2^\circ\text{N}$  (60 cm), and then again increases towards the southern open boundary. The co-range and the co-tidal pattern for  $M_2$  tide shown in Figure 4.30 are similar to the distribution obtained by Rizal [2000]. The decrease in the amplitude of  $M_2$  tide is due to the presence of a virtual amphidromic point. The position of the virtual amphidromic point, as depicted from Figure 4.30, could be located somewhere far inland to the north-east, which is in agreement with the findings of the Rizal [2002]. The distribution of amplitudes of  $S_2$  and  $N_2$  and diurnal tide  $K_1$  tide also shows signatures of virtual amphidromic point. A fine resolution tidal model for Malacca Strait is needed to confirm the presence of virtual amphidromic point.

**Figure 4.30** Detail view of tidal chart of  $M_2$  tidal chart showing co-range and co-phase lines in Malacca Strait.

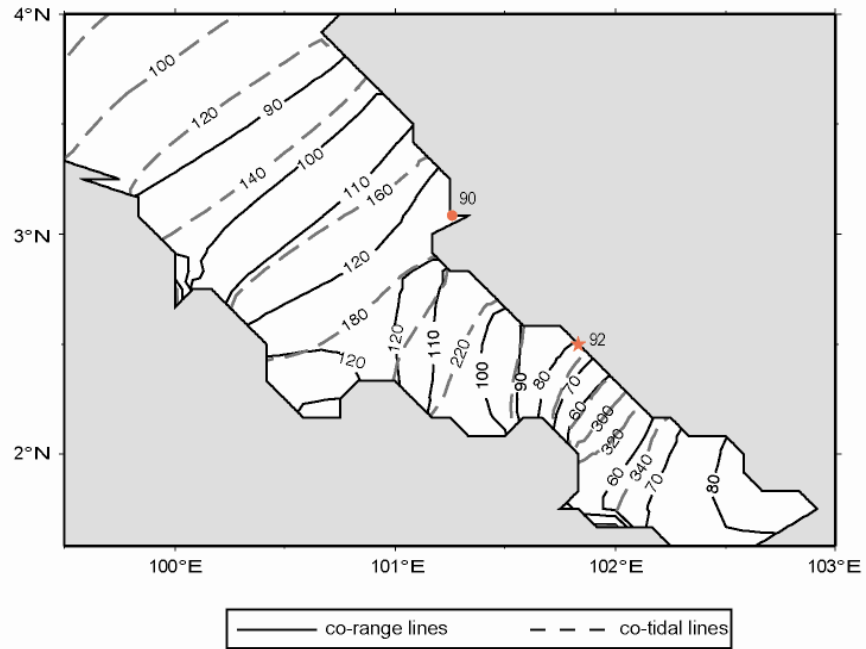
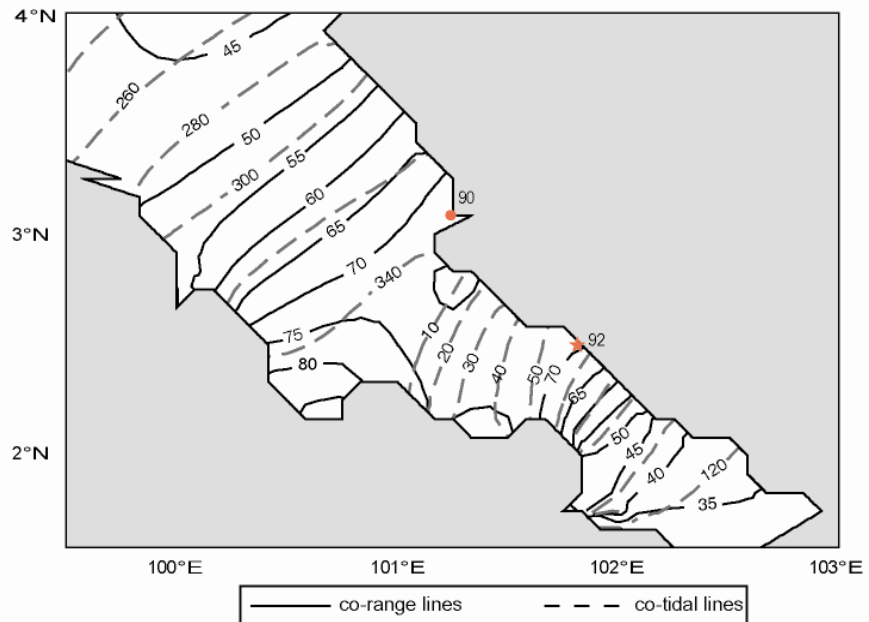


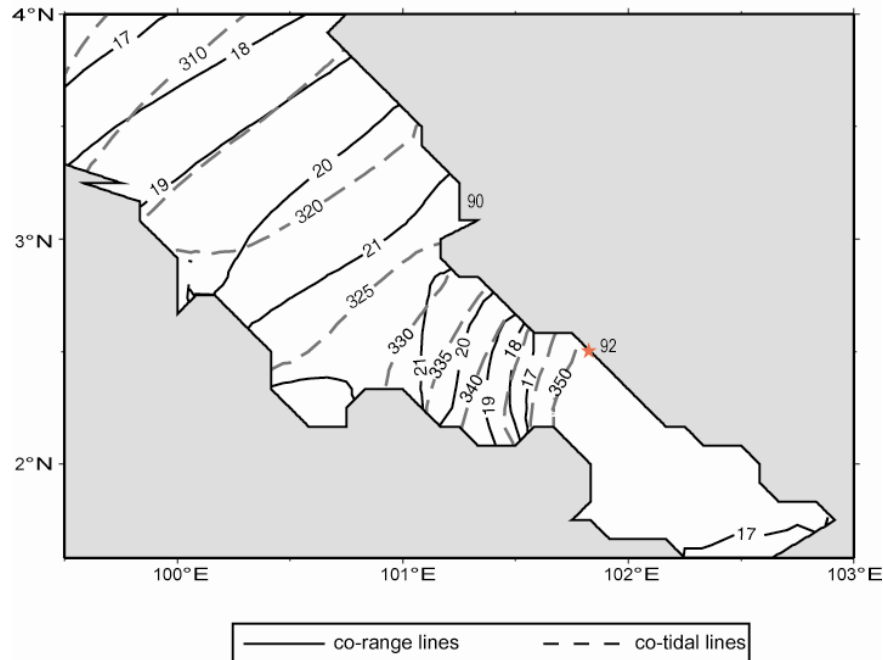
**Figure 4.31** Same as Figure 4.30, but for  $S_2$  tide.



---

**Figure 4.32** Same as Figure 4.30, but for  $K_1$  tide.
 

---



There is a difference in the pattern of the amphidromic points found in the eastern head bay and that in the Malacca Strait. The degenerate amphidromic point observed in the head bay is easily identifiable whereas the Malacca Strait has a purely virtual amphidromic point. This is in accordance to the conclusion of Rizal [2002] who showed that the displacement of the amphidromic systems away from the central axis decreases with the increase in the latitude and therefore the probability of occurrence of virtual amphidromes in higher latitudes is less. It is noted that Rizal and Sundermann [1994] and Rizal [2000] simulated the semi-diurnal constituent  $M_2$  in the Malacca Strait and explained the features exhibited by the  $M_2$  tide in terms of virtual amphidromic point. However, these studies lacked the availability of tidal information along the north western open boundary. The present work, which has the advantage of accurate open boundary conditions, is assessed to provide more accurate results.

## 4.7 Conclusions

A 2D vertically integrated model, developed by Unnikrishnan et al. [1999], was used for the simulation of tides in the Bay of Bengal. The numerical model was thoroughly validated by comparing the simulated composite tides as well as the model derived tidal constituents with observations at different stations covering the entire coastline. The simulated tidal elevations at Paradip, Visakhapatnam and Chennai for a period of 30 days agreed fairly well with the observed tide gauge data, with an RMSE less than 7.5 cm. A reasonable agreement was obtained between the model derived and the observed amplitude and phases of the semi-diurnal and diurnal constituents with RMSE less than 7 cm and 9.5°. It is concluded from the RMS misfit (ORM), being less than 9 cm for all the model derived constituents, that despite the differences between the amplitudes and phases of model derived and observed constituents at a few stations, the model has the capability of reproducing the tidal regime in the area and has sufficient fine grid to capture the near shore tidal variations.

The tidal model was used to simulate each of the major semi-diurnal and diurnal constituents separately in order to develop co-tidal and co-range charts for the constituents  $M_2$ ,  $S_2$ ,  $N_2$ ,  $K_1$  and  $O_1$  for the Bay of Bengal. The characteristic of the tidal constituents in Bay of Bengal and the characteristic features observed in the shallow regions such as head bay, Gulf of Martaban and Malacca Strait were analyzed and illustrated elaborately.

The semi-diurnal tides ( $M_2$ ,  $S_2$ , and  $N_2$ ) are found to amplify nearly twice in the head bay, along the southern coast of Myanmar and in the Gulf of Martaban. The diurnal constituent  $K_1$  amplifies significantly only in the north eastern end of the head bay and in the Gulf of Martaban. The continental shelf in the head bay and along the southern coast of Myanmar is about 200 km wide and the amplitudes of semi-diurnal tides are doubled in these regions while the diurnal tides amplify only marginally, which is consistent with CB theory. In the north eastern end of the head bay and the Gulf of Martaban, the geometrical configuration of the coastline, in addition to the wide continental shelf, could also contribute to the amplification of both semi-diurnal and diurnal constituents. In

the Malacca Strait, the amplitudes of both semi-diurnal and diurnal tides are found to increase gradually from the northern end to the 2.5°N. The highest amplitudes of diurnal tides,  $K_1$  and  $O_1$ , are observed in the Malacca Strait.

The co-tidal and co-range charts of  $M_2$  and  $S_2$  tidal constituents show the presence of two degenerate amphidromic points in the head bay; one in the central part and other in the north eastern end of the head bay. A virtual amphidromic point for  $M_2$  is identified in the Malacca Strait.

The study on the propagation of tides and the distribution of amplitudes and phases of semi-diurnal and diurnal constituents in the Bay of Bengal has been scarce. Therefore, the present study has focussed on the identification of characteristics features in the distribution of major tidal constituents in the Bay of Bengal, especially in shallow regions such as head bay, Gulf of Martaban and Malacca Strait.